1

2

3

4   *Title*:   **Intercellular transmission of a bacterial cytotoxic prion-like**

5   **protein in mammalian cells**

6

7   *Authors*:   Aida Revilla-García[1], Cristina Fernández[1,†], María Moreno-del Álamo[1,†], Vivian

8   de los Ríos[2], Ina M. Vorberg[3], Rafael Giraldo[1, †,*]

9

10   *Affiliations*:   [1] Department of Cellular and Molecular Biology, Centro de Investigaciones

11   Biológicas (CSIC), c/ Ramiro de Maeztu 9, 28040 Madrid, Spain.

12   [2] Proteomics Facility, Centro de Investigaciones Biológicas (CSIC).

13   [3] German Center for Neurodegenerative Diseases (DZNE), Venusberg Campus 1,

14   Building 99, 53127 Bonn, Germany

15

16   * *For correspondence*: rgiraldo@cnb.csic.es

17   * *ORCID Identifier*:   0000-0002-5358-7488

18   † Present address: Dept. of Microbial Biotechnology, CNB-CSIC, C/ Darwin 3, 28049 Madrid

19

22

23

1

1   Abstract

2   RepA is a bacterial protein that builds intracellular amyloid oligomers acting as inhibitory complexes of

3   plasmid DNA replication. When carrying a mutation enhancing its amyloidogenesis (A31V), the N-

4   terminal domain (WH1) generates cytosolic amyloid particles that are inheritable within a bacterial

5   lineage. Such amyloids trigger in bacteria a lethal cascade reminiscent to mitochondria impairment in

6   human cells affected by neurodegeneration. To fulfil all the features of a prion-like protein, horizontal

7   (intercellular) transmissibility remains to be demonstrated for RepA-WH1. Since this is experimentally

8   intractable in bacteria, here we transiently expressed in a murine neuroblastoma cell line the soluble,

9   barely cytotoxic RepA-WH1(WT) and assayed its response to co-incubation with *in vitro* assembled

10   RepA-WH1(A31V) amyloid fibres. In parallel, cells releasing RepA-WH1(A31V) aggregates were co-

11   cultured with human neuroblastoma cells expressing RepA-WH1(WT). Both the assembled fibres and

12   the extracellular RepA-WH1(A31V) aggregates induce, in the cytosol of recipient cells, the formation

13   of cytotoxic amyloid particles. Mass spectrometry analyses of the proteomes of both types of injured

14   cells point to alterations in mitochondria, protein quality triage, signalling and intracellular traffic.

15

16   Summary blurb

17   The horizontal, cell-to-cell spread of a bacterial prion-like protein is shown for the first time in

18   mammalian cells. Amyloid cross-aggregation of distinct variants, and their associated toxicities, follow

19   the same trend found in bacteria, underlining the universality of prion biology.

20

21   Introduction

22   A hallmark of protein aggregates accumulating in human neurodegeneration is their ability to template

23   the conformational change of soluble native protein molecules into highly ordered polymers with a

24   cross-β structure termed amyloid (Eisenberg and Sawaya, 2017; Chiti and Dobson, 2017). This has been

25   extensively characterized for the PrP prion in spongiform proteinopathies (Prusiner, 1998; Aguzzi and

26   Falsig, 2012), the Aβ peptides (Eisele et al., 2010; Stöhr et al., 2012; Watts et al., 2014) and Tau (Frost

27   et al., 2009; Clavaguera et al., 2009; Kfoury et al., 2012; Goedert et al., 2017) in Alzheimer's and

1   related dementias, or α-synuclein in Parkinson's disease (Kordower et al., 2008; Luk et al., 2009; Luk et

2   al., 2012; Prusiner et al., 2015). Protein aggregates are cell-to-cell transmissible through either

3   tunnelling nanotubes, secretion as naked aggregates or packed into extracellular vesicles. These

4   mechanisms underlie the stereotypical spreading of protein aggregates throughout connected brain

5   regions (Polymenidou and Cleveland, 2012; Soto, 2012; Prusiner, 2013; Goedert, 2015; Jücker and

6   Walker, 2018). Such 'horizontal' transmissibility, which partially resembles the infectivity of the PrP

7   prion, qualifies Aβ peptides, Tau and α-synuclein as prion-like proteins (or prionoids) (Aguzzi and

8   Lakkaraju, 2016; Scheckel and Aguzzi, 2018).

9   Intercellular aggregate transmission is not solely a characteristic of disease-associated proteins.

10   Several proteins of lower eukaryotes have the ability to fold into self-templating protein aggregates that

11   faithfully propagate in progeny and transmit to other cells during mating (Wickner et al., 2015).

12   Interestingly, the prion-like behaviour is not restricted to the original host. For example, cell-to-cell

13   propagation of amyloid aggregates has been successfully reported for the NM prion domain of the

14   *Saccharomyces cerevisiae* translation termination factor Sup35 in mammalian cells (Krammer et al.,

15   2009; Hofmann et al., 2013; Liu et al., 2016; Duernberger et al., 2018; Riemschoss et al., 2019). NM-

16   Sup35 can also propagate in bacteria, provided that a specific prion-inducing amyloid required for the

17   prionization of Sup35 in *S. cerevisiae* is also expressed in the recipient cells (Garrity et al., 2010). The

18   other way around, both the amyloidogenic sequence stretch in RepA-WH1 (Gasset-Rosa and Giraldo,

19   2015) and the prion domain in bacterial CbRho (Yuan and Hochschild, 2017) can functionally replace

20   Sup35 prionogenic sequences in a stop-codon read-through translation assay in yeast. However, the

21   transmission of a bacterial prion or prion-like protein to mammalian cells and the assessment of its

22   potential cytotoxicity have not been reported yet. This would complete the demonstration of the

23   universality of the principles governing prion biology.

24   The bacterial prion-like protein RepA-WH1 is a synthetic model of amyloid disease built on RepA, a

25   protein that controls plasmid replication through the assembly of amyloid oligomers that hamper

26   premature rounds of origin firing (Giraldo et al., 2003; Molina-García et al., 2016). The WH1 domain in

27   RepA forms stable dimers in solution. Upon allosteric binding to distinct ligands, dimers dissociate into

28   metastable monomers that subsequently assemble as amyloid oligomers and fibres *in vitro* (Giraldo,

3

1   2007; Torreira et al., 2015). When expressed in *E. coli*, the hyper-amyloidogenic domain variant RepA-

2   WH1(A31V) forms particles of various sizes, distributed across the bacterial cytosol (Fernández-

3   Tresguerres et al., 2010). These particles are transmissible vertically (during cell division, i.e. from

4   mother to daughter cells) as two distinct aggregate strains with remarkable appearances and phenotypes:

5   elongated and mildly cytotoxic, and compact and acutely cytotoxic, respectively (Gasset-Rosa et al.,

6   2014). Co-expression of soluble and aggregation-prone RepA-WH1 variants in *E. coli* demonstrated that

7   the A31V variant can template its conformation on the parental WT protein (Molina-García and

8   Giraldo, 2014). Systems analyses (Molina-García et al., 2017), together with *in vitro* reconstruction in

9   cytomimetic lipid vesicles (Fernández et al., 2016b; Fernández and Giraldo, 2018), suggest that RepA-

10   WH1(A31V) oligomers target the internal bacterial membrane, hampering proton motive force and thus

11   ATP synthesis and transport through membranes, and enhance oxidative stress. In parallel, protein

12   factors mounting the defence against stress and envelope damage co-aggregate with RepA-WH1(A31V)

13   amyloids (Molina-García et al., 2017). Altogether, bacteria viability is severely compromised by RepA-

14   WH1 amyloidosis, in a way resembling some of the central mitochondrial routes found in human

15   amyloidoses (Haelterman et al., 2014; Norambuena et al., 2018; Mathys et al., 2019; Wang et al., 2019).

16   However, *E. coli* is not suitable for addressing the issues of cell-to-cell transmissibility of protein

17   aggregates and the subsequent intracellular amyloid cross-aggregation, since this Gram-negative

18   bacterium does not uptake large protein particles due to the insurmountable obstacle of its three-layered

19   cell envelope.

20   To explore the capability of the prion-like protein RepA-WH1 to propagate in a heterologous host,

21   here we exposed murine neuroblastoma cells, transiently expressing mCherry-tagged soluble RepA-

22   WH1(WT), to *in vitro* assembled RepA-WH1(A31V) amyloid fibres. In addition, we studied the

23   intercellular induction of protein aggregation by co-culturing murine cells releasing RepA-WH1(A31V)

24   aggregates with human neuroblastoma cells stably expressing soluble RepA-WH1(WT). Confocal

25   microscopy and biochemical studies showed that the mammalian cells can take up RepA-WH1(A31V)

26   amyloid fibres, that cross-seed the cytosolic aggregation of the endogenous RepA-WH1(WT) in the

27   recipient cells. Moreover, co-culture of cells releasing the RepA-WH1(A31V) variant also induced the

28   aggregation of RepA-WH1(WT) in bystander cells, suggesting intercellular transmission of RepA-

4

1   WH1(A31V) seeds. In both setups of experimental transmission, the induced RepA-WH1(WT)

2   aggregates were cytotoxic and amyloidogenic in nature, as indicated by cell viability assays and by their

3   affinity for thioflavin-S, respectively. The observed toxicity was dependent on the expression of RepA-

4   WH1(WT) in the recipient cells, suggesting that active assembly of protein aggregates and not simple

5   uptake of toxic polymers was required. This reassures RepA-WH1, whose sequence shows no similarity

6   matches in the human proteome, as a bio-safe prion-like protein. The analyses of the proteomes of either

7   murine cells exposed to the *in vitro* assembled fibres, or human cells internalizing the extracellularly

8   released aggregates, point to the impairment of mitochondria, intracellular trafficking and protein

9   quality control networks in RepA-WH1 toxicity. The results presented here fulfil the validation of

10   RepA-WH1 as a bacterial prion-like protein and reinforce the universality of the molecular and cellular

11   basis of prion biology.

12

13   **Results**

14   **Transient expression in mammalian cells of variants of the RepA-WH1 protein recapitulates their**

15   **aggregation phenotypes in bacteria**

16   Previous findings on the synthetic amyloid proteinopathy elicited in bacteria by the prion-like protein

17   RepA-WH1 suggested that it might have features in common with a wide spectrum of human

18   neurodegenerative amyloidoses. To assess if the model protein RepA-WH1, and its variants exhibiting

19   distinct aggregation propensities in bacteria (Fernández-Tresguerres et al., 2010; Gasset-Rosa et al.,

20   2014; Molina-Garcia et al., 2014), exhibit a comparable behaviour in mammalian cells, proteins were

21   transiently expressed in murine N2a and human SH-SY5Y neuroblastoma cell lines, commonly used in

22   studies about amyloid neurodegeneration, as well as in non-neuronal HeLa cells.

23   RepA-WH1 mutant variants were fused to the monomeric fluorescent protein mCherry in a

24   constitutive expression plasmid (Figure S1A). These fusions, hereafter referred as

25   WH1(WT/A31V/ΔN37)-mCherry for simplification, were the same that had been previously validated

26   regarding their aggregation potential and toxicity in *E. coli* (Fernández-Tresguerres et al., 2010; Gasset-

27   Rosa et al., 2014; Molina-Garcia et al., 2014; Molina-Garcia et al., 2017). While WH1(WT)-mCherry is

28   soluble in the bacterial cytosol and non-cytotoxic, the hyper-amyloidogenic (A31V)-mCherry variant

5

1   aggregates and is highly cytotoxic. WH1(ΔN37) is a deletion mutant lacking the amyloidogenic peptide

2   stretch in RepA-WH1 that forms inclusion bodies. When this mutant is expressed in bacteria, it exhibits

3   reduced toxicity compared to WH1(A31V)-mCherry. Cell lines were transfected with the plasmids

4   coding for RepA-WH1 derivatives, or mCherry as a control. Soluble fractions of cell lysates were

5   analyzed by Western blotting, 48 h after transient transfection, revealing variable protein expression in

6   the three cell lines tested. The highest expression levels were observed in the N2a cells (Figure S1B).

7   Variant WH1(ΔN37)-mCherry was not observed in any cell lysate. The N2a cell line was selected as an

8   appropriate cell background for further exploring RepA-WH1 prion-like behaviour in mammalian cells.

9   As previous work in bacteria had shown that WH1(ΔN37)-mCherry forms massive inclusion bodies

10   (Gasset-Rosa et al., 2014; Molina-Garcia et al., 2014), we explored the presence of this variant in the

11   insoluble lysate fraction of the N2a cells. WH1(ΔN37)-mCherry was clearly located in the pellet,

12   according to Western blot analysis (Figure S1B, right panel), thereby confirming that this mutant also

13   forms insoluble aggregates in the mammalian cytosol.

14   To evaluate the possible cytotoxicity of RepA-WH1, the N2a transfected cells were observed by

15   means of confocal microscopy. As observed in Figure 1A, WH1(WT)-mCherry and the mCherry

16   control remained phenotypically soluble (i.e., they showed diffuse cytoplasmic fluorescence) when

17   overexpressed, which demonstrated that none of them has tendency towards spontaneous aggregation.

18   On the contrary, for the WH1(A31V)-mCherry mutant, small red foci were clearly detected in the

19   cytosol, which correlated with its natural propensity to aggregate in bacteria (Fernández-Tresguerres et

20   al., 2010; Gasset-Rosa et al., 2014; Molina-Garcia et al., 2014). Finally, larger intracellular foci, distinct

21   to those for WH1(A31V)-mCherry, were observed when WH1(ΔN37)-mCherry was expressed.

22   Remarkably, the inspection of nuclei morphology by confocal microscopy revealed the noticeable

23   presence of N2a cells exhibiting a fragmented or condensed nucleus upon WH1(A31V)-mCherry

24   expression, a sign for cell death. This phenotype was rare in cells expressing WH1(WT/ΔN37)-

25   mCherry, or the mCherry control (Figure 1A). Quantitative analysis of the cells showing nuclear

26   condensation/fragmentation at 24, 48 and 72 h after transfection revealed that such difference was

27   statistically significant (Figure 1B). A substantial decrease in the number of WH1(A31V)-mCherry

28   expressing cells was detected at 48 h and, specially, 72 h after transfection, while similar numbers of

6

1   either mCherry control or WH1(WT/ΔN37)-mCherry transfected N2a cells were counted over time.

2   Such reverse correlation between fragmented/condensed nuclei and cell count supports the cytotoxicity

3   of WH1(A31V).

4   To further assess the cytotoxic effect of WH1(A31V)-mCherry overexpression in N2a cells, cell

5   viability was estimated by monitoring the activity of NAD(P)H-dependent oxidoreductases 24, 48 and

6   72 h after transfection (Figure 1C). The MTT reduction assay revealed a decrease in cell viability,

7   compared to the mCherry control, for cells expressing either WH1(A31V)-mCherry or WH1(ΔN37)-

8   mCherry. This toxicity was time-dependent and most pronounced for cells expressing WH1(A31V)-

9   mCherry, resulting in a decrease of cell viability by about 60% at 48 h, to reach 90% at 72 h. On the

10   contrary, no time-dependent changes in cell viability were detected for mCherry and WH1(WT)-

11   mCherry.

12   To verify that the cytotoxic aggregates formed by RepA-WH1 in the N2a cells were of amyloid

13   nature, we relied on thioflavin-S (ThS), an amyloidotropic fluorophore that stains RepA-WH1 amyloids

14   in bacteria (Fernández-Tresguerres et al., 2010; Gasset-Rosa et al., 2014; Giraldo, 2019). Forty-eight

15   hours after WH1(WT/A31V/ΔN37)-mCherry or mCherry transfection, staining with ThS was

16   performed and cells were visualized by confocal microscopy (Figure 2). Image analysis revealed that in

17   the N2a cells expressing WH1(A31V)-mCherry, the aggregated foci were strongly stained by ThS, an

18   indication of their amyloid nature. In contrast, weak, near background ThS staining was observed for

19   cells expressing either the mCherry control, the soluble WH1(WT)-mCherry protein, or for the large

20   WH1(ΔN37)-mCherry aggregates. Reduced binding of the fluorophore was previously considered

21   indicative of the amorphous aggregation of WH1(ΔN37)-mCherry as bacterial inclusion bodies (Gasset-

22   Rosa et al., 2014).

23

24   ***In vitro*-assembled RepA-WH1(A31V) amyloid fibres co-localize with RepA-WH1(WT)**

25   **transiently expressed in the cytosol of murine cells**

26   One of the most remarkable properties of amyloid aggregates is their inherent self-propagation potential,

27   being able to template the amyloid conformation on soluble molecules of the same protein. For RepA-

28   WH1 this had been shown in *E. coli in vivo* by co-expressing WH1(A31V) and WH1(WT) labelled with

7

1   different fluorescent proteins (Molina-García and Giraldo, 2014). Thereby, validation of RepA-WH1 as

2   a 'generic' model for amyloidosis required testing its ability to cross-seed aggregation within

3   mammalian cells.

4   We explored whether exogenous, *in vitro* assembled WH1(A31V) fibres (Figure S2), whose amyloid

5   nature has been well established (Giraldo, 2007; Fernández-Tresguerres et al., 2010; Moreno del Álamo

6   et al., 2015; Torreira et al., 2015; Fernández et al., 2016a), could trigger the aggregation of the otherwise

7   soluble WH1(WT) protein (Figure 1A, second row) in the cytosol of mammalian cells. To this aim, N2a

8   cells transiently expressing WH1(WT)-mCherry in the cytosol were exposed to *in vitro* pre-assembled

9   WHI(A31V)-Alexa 488 labelled amyloid fibres (for simplification, hereafter WH1(A31V) fibres)

10   (Figure 3A). These were mechanically fragmented before incubation with cells to get fibre sizes more

11   suitable for their uptake (see Materials and Methods) (Figure S2). To check for the specific requirement

12   of the WH1(WT) domain as the target for aggregation templating by WH1(A31V) fibres, control cells

13   expressing just mCherry were incubated with the fibres in parallel. Confocal microscopy sections

14   revealed that the WH1(A31V) fibril particles were efficiently internalized by the N2a cells expressing

15   either mCherry or WH1(WT)-mCherry (Figure 3B). In the latter, fibrils co-localized with the

16   endogenous WH1(WT)-mCherry in small, dot-like cytosolic aggregates (Figure 3B, arrows).

17   Approximately 70% of the WH1(WT)-mCherry expressing cells displayed red puncta upon incubation

18   with the fibres, while spontaneous foci formation of WH1(WT)-mCherry was detected in < 35% of the

19   cells after 48 h (Figure 3C). These figures significantly differed from < 20% of foci-bearing cells

20   counted for the mCherry control, irrespective of the presence or absence of added fibrils (Figure 3C).

21   Overall, these observations support that induction of foci by WH1(A31V) amyloid fibres requires

22   expression of a homologous protein substrate in the recipient cells.

23   As a consequence of amyloid templating, it can be assumed that the foci induced in mammalian cells

24   by the internalized amyloid fibres are amyloid aggregates. In order to qualitatively assess this point, ThS

25   staining was performed (Figure 4). Confocal microscopy images obtained after 48 h of fibre addition to

26   the cell cultures revealed the selective binding of ThS to the induced cytosolic WH1(WT)-mCherry

27   aggregates. On the contrary, no intense ThS staining was observed for cells expressing mCherry,

28   attributable to background fluorescence. These findings are compatible with the results of ThS binding

8

1   to the intracellular aggregates generated upon transient expression of WH1(A31V)-mCherry (Figure 2).

2   Therefore, ThS staining provides evidence for the amyloid nature of the WH1(WT)-mCherry aggregates

3   as templated by the WH1(A31V) fibres in the cytoplasm of murine N2a cells.

4

5   RepA-WH1(A31V) released from murine cells can cross-seed amyloid aggregation in the cytosol

6   of recipient human cells stably expressing RepA-WH1(WT)

7   The studies described above provided evidence for the ability of WH1(A31V) to cross-seed WH1(WT)

8   amyloidogenesis in the cytosol of mammalian cells. To further explore this, we aimed to generate stable

9   donor cell lines in which the WH1 variants and controls, fused to the green fluorescent protein

10   TagGFP2, could be expressed under an inducible promoter (pTRE3G Tet-ON vector, genome-

11   integrated THN-rtTA transactivator; see Materials and Methods) (Figure S3A). We chose SH-SY5Y as

12   the parental donor cell line as transgene expression in that background was less pronounced than in N2a

13   cells (Figure S1B). Unfortunately, we were unable to get any clone expressing WH1(A31V)-TagGFP2,

14   suggesting that, even under a tightly regulated gene expression, any transcriptional leak of this mutant

15   variant results in acute cytotoxicity. For the WH1(WT)-TagGFP2 and the control TagGFP2 constructs,

16   efficient doxycycline (Dox)-induced expression was verified through Western blot (Figure S3B) and

17   flow cytometry (Figure S3C) analyses. Confocal microscopy imaging indicated that both the THN-

18   rtTA/WH1(WT)-TagGFP2 and THN-rtTA/TagGFP2 double-stable clones showed an homogeneous,

19   diffuse expression throughout the entire cytosol (Figure S3D).

20   The horizontal, cell-to-cell spreading of RepA-WH1, a key feature to qualify it as a prion-like

21   protein (Aguzzi and Lakkaraju, 2016), was then explored. To this aim, murine N2a donor cells

22   transiently expressing either WH1(A31V)-mCherry or WH1(WT)-mCherry (Figure 1A) were co-

23   cultured with THN-rtTA/WH1(WT)-TagGFP2 recipient cells, which stably expressed soluble

24   WH1(WT)-TagGFP2 upon Dox addition (Figure S3D), for a period of up to a week (Figure 5A). To

25   control for non-specific spontaneous aggregation in the human cells, recipient cultures not mixed with

26   donors were similarly processed in parallel. The formation of foci in the recipient cells was assessed by

27   confocal microscopy imaging every 24 h (Figure 5B,C, left). Noticeably, small green fluorescent puncta

28   were detected over time in the THN-rtTA/WH1(WT)-TagGFP2 recipient cells when the donor N2a cells

1   expressing the hyper-amyloidogenic variant WH1(A31V)-mCherry were added, peaking at 5 days

2   (Figure 5C, left-bottom) and decreasing thereafter, which suggests killing of the cells. On the contrary,

3   no substantial formation of WH1(WT)-TagGFP2 foci was observed upon addition of the N2a donors

4   transiently expressing WH1(WT)-mCherry (Figure 5C, left-top) to the human recipient cells.

5   Fluorescent puncta were not apparent either for their control counterparts, in which donors expressing

6   WH1(A31V/WT)-mCherry were added to cultures of recipient cells THN-rtTA/TagGFP2 (Figure 5B,

7   left). These results fully parallel (and strengthen) the observations made when exogenously added, *in*

8   *vitro*-assembled WH1(A31V) fibres induced the formation of WH1(WT)-mCherry foci in the N2a cells

9   (see above; Figure 3). Five days co-cultures were selected for quantitative image analysis of the fraction

10 of cells that exhibited green fluorescent foci. Just 10-12% of the human control cells endogenously

11 expressing TagGFP2 showed some fluorescent spots, irrespective of being co-cultured with murine cells

12 expressing WH1(A31V)-mCherry or WH1(WT)-mCherry. Puncta were apparent in ≈35% of the

13 recipient cells expressing WH1(WT)-TagGFP2 only if the hyper-amyloidogenic WH1(A31V)-mCherry

14 variant was expressed by the donor murine cells (Figure 5B,C, right).

15   While WH1(A31V)-mCherry aggregates must be first released (either through exocytosis or, more

16 likely, upon cell death) to the culture medium from the donor cells and subsequently gain access into the

17 recipient cells, it is noteworthy that red fluorescent WH1(A31V)-mCherry particles were rarely detected

18 at the intercellular space. Although it is possible that the loss of such particles may occur during the

19 manipulation of the samples (e.g., for cell passages or microscopy), the most likely explanation is that

20 their size range is beyond the resolution of conventional confocal imaging (Hofmann et al., 2013; Liu et

21 al., 2016).

22   In conclusion, these results showed significant differences in the intercellular 'infectivity' of soluble

23 WH1(WT)-mCherry and hyper-amyloidogenic WH1(A31V)-mCherry. Cells suffering from the RepA-

24 WH1(A31V) amyloidosis were highly proficient in the propagation of an aggregation-related

25 phenotype, which was consistent with the results obtained for the *in vitro* pre-assembled RepA-

26 WH1(A31V) fibrils. Altogether, these parallel observations suggest that the bacterial RepA-WH1

27 protein indeed follows in mammalian cells a prion-like mechanism for horizontal transmission.

28

10

1   **A proteomic outline of the cytotoxicity of RepA-WH1(A31V) amyloids in mammalian cells**

2   In a previous study, we characterized the systems-wide response of *E. coli* to WH1(A31V)-mCherry

3   expression to identify pathways potentially affected by the bacterial amyloidosis (Molina-García et al.,

4   2017). To assess cellular responses to the toxic WH1(A31V) amyloids, we performed parallel proteomic

5   studies on three groups of samples: i) N2a cells transiently expressing WH1(WT)-mCherry or mCherry,

6   collected after 48 h of incubation with WH1(A31V) fibres (see Figure 3; Supplemental Dataset 1); ii)

7   THN-rtTA/SH-SY5Y cells expressing WH1(WT)-TagGFP2 or TagGFP2, harvested after 5 days of

8   induction with Dox in co-culture with N2a cells expressing WH1(A31V)-mCherry (see Figure 5;

9   Supplemental Dataset 2); and iii) control naïve N2a or THN-rtTA/SH-SY5Y cells incubated,

10   respectively, with WH1(A31V) fibres or WH1(A31V)-mCherry donor cells.

11   The subsets of the proteomes that were exclusively found in recipient cells expressing WH1(WT)-

12   mCherry (N2a cells, mice) or WH1(WT)-TagGFP2 (THN-rtTA/SH-SY5Y cells, human), and not in

13   cells just expressing their respective fluorescent tag controls, upon fibre-induced or cell-to-cell spread of

14   amyloidogenesis reflect a broader response for latter experimental scenario (Figures 6 and S4). Albeit

15   the individual proteins identified are not the same (perhaps also due to host species-specific features),

16   both datasets point to shared pathways affected in the RepA-WH1 amyloidosis. These include distinct

17   subcellular organelles, specially mitochondria and the endoplasmic reticulum, and processes, among

18   which metabolism and signalling are the most frequent hits. Cluster analyses further refine these

19   findings, confirming that mitochondria are at the very core of the RepA-WH1 amyloidosis under both

20   experimental approaches (Figure S4), with Complex I of the respiratory chain (NADH:ubiquinone

21   oxidoreductase) as the most prominent node. In addition, protein quality control machinery (the

22   proteasome, ubiquitin-ligases and chaperones), cell signalling and intracellular trafficking networks,

23   linked to protein secretion, are affected by WH1(A31V) uptake.

24   Interestingly, similarities between the response of mammalian mitochondria to amyloid-promoted

25   neurodegeneration and how *E. coli* reacts to RepA-WH1 amyloidosis were previously proposed on the

26   basis of systems analyses carried out in the latter host (Molina-García et al., 2017). The results

27   presented here reinforce this view and make sense in light of the common ancestry of Gram-negative

1   bacteria and mitochondria, validating RepA-WH1 as a minimal, autonomous proxy to sketch core

2   mitochondrial routes involved in human amyloidoses.

3

4   **Discussion**

5   The ability of highly ordered protein aggregates to intercellulary template their amyloid structure on

6   soluble molecules of the same protein found in naïve recipient cells has recently emerged as a hallmark

7   of human neurodegenerative diseases. In common with the infectious propagation of the PrP prion, cell-

8   to-cell transmission of prion-like protein aggregates has been established for α-synuclein, Tau, Aβ

9   peptides, and it is now being explored for many other proteins involved in neurodegeneration

10   (Polymenidou and Cleveland, 2012; Soto, 2012; Prusiner, 2013; Goedert, 2015; Jücker and Walker,

11   2018). The proteins involved in such aggregation cross-seeding *in vivo* are thus considered prion-like

12   proteins or prionoids (Aguzzi and Lakkaraju, 2016; Scheckel and Aguzzi, 2018). In these cases, the

13   intercellular traffic is likely mediated by generation of extracellular vesicles from the donor cells and

14   subsequent endocytic uptake by the recipient cells (Liu et al., 2016).

15   RepA-WH1 is a bacterial prion-like protein that recapitulates in *E. coli* many of the essential features

16   of an amyloid proteinopathy, including the formation of cytotoxic amyloid aggregates (Fernández-

17   Tresguerres et al., 2010; Molina-García et al., 2017), the existence of strains that give rise to distinct

18   phenotypes, and their epigenetic vertical (mother-to-daughter cells) transmission coupled to cell

19   division (Gasset-Rosa et al., 2014). However, its ability to be horizontally (cell-to-cell) transmitted as a

20   prion-like protein had not been addressed yet in bacteria, due to the stringent barrier that to the uptake of

21   large protein aggregates impose the peptidoglycan and, in Gram-negative bacteria, also the outer

22   membrane. We have now used mammalian cultured cells and fluorescent-labelled proteins to address

23   the issue of the horizontal transmissibility of RepA-WH1. We first transiently expressed distinct

24   variants of RepA-WH1 in murine cells, which led to the formation of amyloids with similar degrees of

25   cytotoxicity to those described in bacteria, i.e., WH1(A31V) >> WH1(ΔN37) > WH1(WT) (Gasset-

26   Rosa et al., 2014; Molina-García et al., 2017). Then incubation of those cells with *in vitro*-assembled

27   amyloid WH1(A31V) fibres showed their ability to induce the formation of foci by WH1(WT), which is

12

1   otherwise soluble as expressed in the cytoplasm of the recipient cells. In a subsequent step, we

2   generated a stable and inducible cell line expressing soluble WH1(WT), which assembled as fluorescent

3   puncta upon exposure to WH1(A31V) particles generated by donor cells. The results from these

4   experiments fulfil the last stalling requirement to qualify RepA-WH1 as a prion-like protein: its ability

5   to be horizontally transmissible.

6   It is noteworthy that, under our experimental conditions, the uptake of recombinant WH1(A31V)

7   amyloids by cells not expressing WH1(WT), but just the fluorescent proteins to which the prion-like

8   protein was tagged, does not result in any evident toxicity for the recipient cells. Although there is no

9   protein with a noticeable degree of sequence identity with RepA-WH1 in the human proteome (BLAST

10   best match E-value = 0.11), it has been recently suggested that bacterial extracellular amyloids may

11   template amyloidogenesis on human proteins implicated in neurodegeneration in spite of the lack of

12   significant sequence similarities (Friedland and Chapman, 2017; Perov et al., 2019). This could

13   constitute a matter of concern on the biosafety of bacterial amyloids. In contrast, the inability of

14   WH1(A31V) amyloids to induce either intracellular aggregation or toxicity in naïve mammalian cells

15   not expressing RepA-WH1 qualifies this protein as biosafe.

16   In the context of the experiment in which amyloidogenesis was induced by adding exogenous fibres,

17   it is most relevant that the intracellular foci in the recipient cells were templated by a well characterized

18   amyloid structure assembled *in vitro* (Giraldo, 2007; Torreira et al., 2015), which in turn was seeded by

19   intracellular aggregates extracted from *E. coli* cells experiencing WH1(A31V) amyloid toxicity

20   (Fernández-Tresguerres et al., 2010). Therefore, it can be assumed (Luk et al., 2009; Stöhr et al., 2012;

21   Lu et al., 2013; Frederick et al., 2014; Qiang et al., 2017) that the intracellular amyloid (ThS-reactive)

22   foci in the recipient murine cells may have the same intimate structure as the aggregates reported to kill

23   bacterial cells.

24   The toxicity of the amyloid proteins involved in neurodegeneration can be due to the loss, on their

25   aggregation, of an essential cellular function and/or to the gain of an emergent functionality by the

26   aggregates (Chiti and Dobson, 2017), e.g., upon the assembly of oligomeric membrane pores

27   (Fernández et al., 2016b). In the case of the phenotype caused in the mammalian cells by the expression

28   of WH1(A31V) amyloids (Figures 1 and 2), or by their uptake and subsequent templating on WH1(WT)

1 in the recipient cells (Figures 3-5), cytotoxicity is necessarily an intrinsic property of the aggregates

2 themselves, because *a priori* no function is associated with this bacterial prion-like protein in the

3 heterologous mammalian host. Very recently, RepA-like proteins with a conserved WH1 domain (Kilic

4 et al., 2019) have been described as nearly the only gene products encoded by small mobile genetic

5 elements that were isolated in dairies and meat (BMMFs), with a probable origin in cattle microbiota,

6 but also in samples from patients with cancer and multiple sclerosis (de Villiers et al., 2019). These

7 findings open the intriguing possibility that the cytotoxicity described here for RepA-WH1 might have

8 broader relevance in human disease.

9 Mass spectrometry analyses of the proteins specifically detected upon the uptake of RepA-

10 WH1(A31V) under the two main scenarios of experimental transmission addressed (Figure 6) provided

11 a picture sharing some similarities to cells in neurodegeneration. In the case of exogenous nucleation of

12 WH1(WT) amyloids by WH1(A31V) fibres, proteins annotated as involved in neurodegenerative

13 diseases were identified (Crat, Hexb, Pld3 and Sel1l), while others were related to ubiquitin ligases and

14 proteasome-mediated degradation pathways (Fbxo2 and Isg15). Upon the uptake of secreted/released

15 WH1(A31V) particles, proteins linked to neurodegeneration (Arsa, Epm2aip1 and Hm13) also showed-

16 up, together with co-chaperones (Chordc1, Dnajb4 and Dnajc11) and proteins involved in vesicular

17 trafficking (Arfgap2, Copb2, Dis3 and Flot1) or in apoptosis (Bak, Cul1, Ier3ip1, Mfge8, Psmd6, Tpp2

18 and Stk4). It is noteworthy that the latter participates in chromatin condensation, as observed in Figure

19 1B. Mitochondrial proteins as well as those located at the endoplasmic reticulum were the most

20 common hits, preferentially proteins directly related with bioenergetics (respiratory chain) and with

21 secretory pathways, respectively. Two proteins are worth noting in the context of what is known on

22 RepA-WH1(A31V) toxicity in *E. coli*: Apool, which binds to cardiolipin, the bacterial and

23 mitochondrial-specific acidic phospholipid that promotes the formation of pores by the prionoid in

24 model membranes (Fernández et al., 2016b), and Romo1, a protein that enhances the formation of

25 reactive oxygen species (ROS) in mitochondria, usually as an anti-microbial response. Romo1 might be

26 playing the same role, albeit through a different mechanism, that the auto-oxidation of the alternative

27 dehydrogenase NdhII plays in bacteria, i.e., constituting the first step in the oxidative cascade leading to

28 cell death (Molina-García et al., 2017). Attempts to counteract ROS generation in mitochondria seem to

14

1   rely on Nnt, which generates NADPH and thus reduction power to detoxify free radicals. Interestingly,

2   a central role in the cytotoxicity of the PrP prion has been proposed for NADPH oxidases (Sonati et al.,

3   2013).

4   Several systems analyses, based on differential transcriptomics and proteomics, have been reported

5   for conditions related to neurodegenerative amyloidoses (Hwang et al., 2009; Olzscha et al., 2011; Hosp

6   et al., 2015; Woerner et al., 2016; Kim et al., 2016; Seyfried et al., 2017; Markmiller et al., 2018;

7   Mathys et al., 2019). One-third of the proteins identified in our analysis (Figure 6) were also found

8   among the genes overexpressed, or the proteins captured within aggregates, in those datasets, thus

9   defining a subset of proteins (Table S1) distinctive of a 'generic' cellular model of amyloidosis, as it can

10   be outlined with the synthetic bacterial prion-like RepA-WH1 protein.

11

Materials and Methods

Plasmid Constructions

Generation of the pcDNA3.1 vectors

15   The gene fusions *repA-WH1(WT)-mCherry*, *repA-WH1(A31V)-mCherry* and *repA-WH1(ΔN37)-*

16   *mCherry*, or *mCherry* were amplified by PCR (5´-CCGGGTACCATGGGCAGCAGCCATCATC and

17   5´- CGGGAATTCTTACTTGTACAGCTCGTCCAT primers; Pfu DNA polymerase, Promega) from

18   the pRG*rectac*-NHis constructions (Fernández-Tresguerres et al., 2010). The PCR products were cloned

19   into pcDNA3.1 (Invitrogen) after cutting with KpnI (5´end) and EcoRI (3´end) (Fig. S1A). Constructs

20   were screened by colony PCR and restriction enzyme digestion, and confirmed by Sanger sequencing

21   (Secugen: https://www.secugen.es).

Generation of the pTRE3G vectors

23   For generation of SH-SY5Y stable cell lines expressing WH1(WT)-TagGFP2, or TagGFP2 as a control,

24   the *TagGFP2* sequence of the pTagGFP2-N vector (Evrogen) was amplified via PCR (5'-

25   ATAAGAATTCCGGAATGAGCGGGGGCGAGGAG and 5'-

26   CGGGGAATTCCATATGTTACCTGTACAGCTC primers) and cloned into pcDNA3.1-mCherry (see

27   above) via BspEI and EcoRI digestions, thus replacing the red by the green fluorescent protein. The

1   RepA-WH1(WT) domain was then excised form pcDNA3.1-*WH1(WT)-mCherry* and fused in frame

2   with TagGFP2 by digestion with SacII and BspEI.

3   For the Tet-ON inducible expression plasmid pTRE3G (Clontech), *WH1(WT)-TagGFP2* and *TagGFP2*

4   genes were amplified by PCR (5´-GAAGATCTATGGGCAGCCATCATCATCA and 5´-

5   CCGGAATTCCATATGTTACCTGTACAGCCTC primers). The amplified PCR fragments were

6   subcloned into pTRE3G with BglII and NdeI to obtain pTRE3G-*TagGFP2* and pTRE3G-*WH1(WT)-*

7   *TagGFP2* (Fig. S3A).

8   **Generation of pET-*WH1(A31V,K132C)***

9   For labelling the protein RepA-WH1(A31V) with Alexa Fluor 488, a variant with only one cysteine was

10   constructed. The gen *repA*-WH1(A31V) was amplified from a mutant variant in which Cys29 and

11   Cys106 had been replaced by serines (Diederix et al., 2008), and a new C-terminal cysteine was added

12   replacing Lys in position 132, using the following primer: 5'-

13   GCTAAGCTTCAACAGAGCTGATAGCTGGTGAACTC. The *repA-WH1(A31V,K132C)* gene

14   was interchanged with the insert in pET3d-*repA-WH1* (Fernández and Giraldo, 2018) upon digestion

15   with SacII and BamHI.

16

17   **Protein Biochemistry**

18   **RepA-WH1(A31V) protein purification**

19   The RepA-WH1(A31V) protein used in the fibrillation studies was purified as described in (Giraldo,

20   2007). RepA-WH1(A31V, K132C) was expressed in *E. coli* BL21(DE3) bearing pET-

21   *WH1(A31V,K132C)*, plus pLysS to enable endogenous lysozyme-promoted lysis after freezing–thawing.

22   Cells were grown in Terrific Broth medium supplemented with ampicillin (Ap) to 100 µg·ml^{-1} at 30 ºC

23   to an OD_{600nm} of 0.8. Then, IPTG was supplied to 0.5 mM and expression proceeded for 6 h at room

24   temperature (RT). Cells were harvested and protocol was followed as described (Giraldo, 2007). The

25   concentration of purified protein was determined by absorption at 280 nm (ε^{280} = 11,548 M^{-1}·cm^{-1}).

26   **Fluorescent labelling of RepA-WH1**

1   The single cysteine residue in RepA-WH1(A31V,K132C) was labelled with Alexa Fluor 488 maleimide

2   (Invitrogen) using thiol chemistry. Briefly, the protein (~50 µM) was dialyzed against 20 mM of sodium

3   phosphate buffer pH 7.0 and 100 mM Na_2SO_4. After dialysis, TCEP [tris(2-carboxyethyl) phosphine-

4   hydrochloride] to 2 mM and urea to 2 M were added and incubated for 1 h on ice. TCEP maintains the

5   cysteine residue in a reduced form, available for derivatization. The fluorophore was prepared by

6   dissolving 250 µg in 10 µl H_2O and added dropwise to the protein solution while gently agitated in a

7   small vial. We used 5-fold molar excess of the dye to protein at 50 µM. From this point onwards, the

8   sample was protected from light using aluminium foil. The conjugation reaction was allowed to proceed

9   at RT for 4 h under mild agitation. After protein labelling, unconjugated Alexa Fluor 488 was separated

10   in a 5 mL desalting column (GE Healthcare). Sample was divided into aliquots, flash frozen in N_2(l),

11   and stored at -70°C after adding glycerol to 10%. Each aliquot was thawed immediately before the

12   experiment and used only once. The fraction of protein labelled was 20% (i.e., ~0.2 moles of dye per

13   mole of protein).

14   **Fibre assembly**

15   Fibres were prepared with a modification of the protocol described in (Giraldo et al., 2007; Torreira et

16   al., 2015). 25 µM of RepA-WH1(A31V) and 0.5 µM of Alexa 488-labelled RepA-WH1(A31V,K132C)

17   were mixed in a final reaction volume of 100 µl of 0.1 M Na_2SO_4, 4 mM $MgSO_4$, 40 mM HEPES pH 8

18   and 7% PEG-4000. 1 µl (diluted 1:100 from the stock) of purified intracellular RepA-WH1(A31V)-

19   mCherry inclusions were added to nucleate amyloid assembly (Fernández-Tresguerres et al., 2010).

20   Fibres were formed in 500 µl Eppendorf tubes at 4°C for 20 days. For cellular uptake experiments,

21   fibres were centrifuged at 13,000 rpm for 30 min. After centrifugation, the supernatant was removed and

22   fibres were washed with buffer (50 mM Na_2SO_4, 40 mM HEPES pH 8) and centrifuged again to be

23   finally resupended in the same buffer. To get a more efficient internalization, immediately before

24   incubation with cells, fibres were fragmented by 5 min sonication in a water bath (Ultrasonic cleaner

25   USC100T, 60W), and further broken up by pipetting with a 100 µl Hamilton syringe for 2 min. Fibres

26   were checked by means of electron microscopy (Fig. S2A), as indicated in (Giraldo, 2007; Fernández et

27   al., 2016b), and confocal microscopy (Fig. S2B; see below). The size distribution of the fibres as added

28   to the cell cultures was 257.6 ± 188.0 nm (n= 243).

1   **Whole cell protein extraction**

2   Either transiently transfected N2a or stable SH-SY5Y cells (see below) were rinsed in PBS, detached by

3   scraping and harvested by centrifugation at 2,000 rpm, for 5 min at 4ºC. Cell pellets were resuspended

4   in 100 μl of RIPA buffer (Sigma), supplemented with protease and phosphatase inhibitors (Roche),

5   incubated on ice for 30 min and then centrifuged at 14,000 rpm for 5 min at 4 ºC. Pellets and

6   supernatants were kept frozen at -80ºC. Cell lysate supernatants were denatured with Laemmli buffer

7   for 5 min at 95 ºC and samples were loaded (30 μg total protein per lane) onto 12.5% SDS-denaturing

8   polyacrylamide gels. Western blot analysis was performed after semi-dry transference of SDS-PAGE

9   gels to PVDF membranes, using mouse anti-GFP (1:1,000; Abcam), or rabbit anti-mCherry (1:5,000;

10 Abcam) antibodies, and anti-actin (1:1,000; Abcam) or anti-vinculin (1:1,000; Sigma) antibodies as

11 loading controls. Then membranes were incubated with HRP-conjugated secondary anti-mouse/rabbit

12 antibodies (1:10,000; Sigma). Blots were developed with ECL (Pierce).

13

14 **Cell Biology**

15 **Cell cultures**

16 The murine neuroblastoma cell line Neuro 2a (N2a; DSMZ-Germany), and the human HeLa (DSMZ)

17 and neuroblastoma SH-SY5Y (CIB-CSIC stock) cell lines were cultured in Dulbecco's Modified Eagle

18 Medium: nutrient Mixture F-12 (DMEM-F12) (Gibco) supplemented with 10% tetracycline-free fetal

19 bovine serum (FBS) (Capricorn), 200 mM glutamine (Gibco) and 1% penicillin/streptomycin (Gibco).

20 For the selection and maintenance of SH-SY5Y stable clones, geneticin (Gibco) and hygromycin B

21 (Clontech) were added to the medium. Tet-ON expression was induced by doxycycline (Sigma). Cells

22 culture was carried out at 37 ºC in a humidified 5% CO_2 incubator. Every 3-4 days, cells were grown to

23 near confluence (80-90% density) and then detached using 0.05% trypsin-EDTA (Gibco) for

24 subculturing.

25 **N2a cells transfection**

26 N2a cells were transiently transfected at ≈70% confluence in a 6-well plate by adding per well 10 μL

27 Lipofectamine 2000 (Invitrogen) together with 3 μg of the respective pcDNA3.1 plasmid derivative.

18

1   DNA-Lipofectamine complexes were prepared according to the manufacturer´s protocol in serum-free

2   DMEM-F12 medium. Protein expression was followed by Western-blot analysis (Fig. S1B; see above)

3   and confocal microscopy (see below).

4   **Uptake of amyloid fibrils by N2a cells**

5   To assay the uptake of the *in vitro* pre-assembled RepA-WH1(A31V)-Alexa 488 labelled fibres by the

6   N2a cell line, cells were seeded in 35 mm plates and transiently transfected with pcDNA3.1-*repA-*

7   *WH1(WT)-mCherry*, expressing a soluble variant of RepA-WH1 (Fernández-Tresguerres et al., 2010;

8   Molina-García and Giraldo, 2014), or pcDNA3.1-*mCherry* as a control (see above; Fig. S1A).

9   Immediately after transfection, N2a cells were exposed to RepA-WH1(A31V)-Alexa 488 fibres (1 μM

10   in equivalent protein monomers) in the growth medium. Next day, cells were extensively rinsed with

11   PBS and further cultured in fresh medium. Fluorescence was subsequently monitored by confocal

12   microscopy 24, 48 and 72 h after the exposure to the fibres.

13   **Generation of stable and Tet-ON regulated expression cell lines**

14   To stably express RepA-WH1(WT)-TagGFP2 and TagGFP2 in the SH-SY5Y cell line, the Tet-ON 3G

15   expression system (Clontech) was used. It is composed of pCMV-*Tet3G* (regulatory) and pTRE3G

16   (response) plasmids. To generate SH-SY5Y cells expressing the trans-activator protein (rtTA) upon

17   genomic integration of pCMV-*Tet3G*, 1 μg of this plasmid was transfected into $5x10^5$ SH-SY5Y cells

18   with Lipofectamine LTX PLUS (1:1 ratio; Invitrogen) and selected for colonies with G418 (0.5 mg/ml).

19   Individual clones, isolated using a cloning cylinder (Sigma), were then screened for luciferase activity

20   (see below). Suitable THN-rtTA/SH-SY5Y clones (i.e., those with high luciferase induction and low

21   basal expression) were subsequently co-transfected with a mixture (10:1) of pTRE3G-*WH1(WT)-*

22   *TagGFP2* (or pTRE3G-*TagGFP2*) and a hygromycin linear selection marker. Double-stable SH-SY5Y

23   transfectants were then selected by screening with hygromycin (0.4 mg/ml) and G418 (0.5 mg/ml) for 2

24   weeks, testing for the best expression of *repA-WH1(WT)-TagGFP2* and *TagGFP2* genes in the

25   presence/absence of doxycycline (0.5 μg/ml) after 48 h by Western-blot (Fig. S3B; see above), flow

26   cytometry (Fig. S3C) and confocal microscopy (Fig. S3D) (see below).

27   **Luciferase assay**

28   The luciferase assay kit (Promega) was used to test the expression and regulation performance of the

19

1   selected transactivator-positive clones. Specifically, G418 resistant THN-rtTA/SH-SY5Y clones were

2   seeded in a 6-well culture plate at a density of $5x10^5$ cells/well. One day after seeding, cells were

3   transiently transfected with 5 µg of the pTRE3G-Luc control vector (Clontech) using Lipofectamine

4   LTX (see above). Luciferase expression was induced by adding 0.5 µg/ml doxycycline for 48 h to

5   complete DMEM-F12 medium. In parallel, to test clones for basal luciferase expression, controls with

6   no doxycycline supplied were casted. Thereafter, cells were harvested in RIPA lysis buffer and

7   bioluminescence was monitored at 562 nm using a TD-20/20 Turner Designs luminometer.

8   **N2a/SH-SY5Y co-cultures**

9   To explore cell-to-cell transmissibility of protein particles, SH-SY5Y stable cells (recipient cells),

10   expressing either soluble WH1(WT)-TagGFP2 or TagGFP2, were seeded on glass coverslips coated

11   with 0.1 mg/ml poly-L-lysine (Sigma) and casted in 24-well plates. Twenty-four h afterwards, N2a cells

12   (donor cells) transiently transfected with pcDNA3.1-*WH1(A31V)-mCherry* or pcDNA3.1-*WH1(WT)-*

13   *mCherry* were detached with trypsin and transferred to the plates bearing the SH-SY5Y receptor cells

14   (2:1 ratio) and co-cultured for 5 days in DMEM-F12 completed media with 0.5 µg/ml doxycycline.

15   Cells were then fixed with 4% p-formaldehyde (PFA) during 15 min and stained with DAPI (5 min, 1

16   µg/ml in PBS; Merck-Millipore).

17   **Flow cytometry**

18   Flow cytometry was used to monitor fluorescent protein expression in the stable clones for rtTA

19   transactivator, either in the presence or absence of 0.5 µg/ml doxycycline, at 48 h after induction. Cells

20   were detached by trypsinization from 35 mm culture dishes and centrifuged at 1,000 rpm for 5 min at

21   4ºC. Then, pellets were resuspended in 2 ml of cold PBS buffer. GFP (Excitation/Ex 488 nm;

22   Emission/Em 525 nm) fluorescence was measured in a Coulter Epics XL (Beckman-Coulter) flow

23   cytometer, analysing 10,000 cells per sample. Subsequent data analysis was performed using the

24   Flowlogic software (v7.2.1).

25   **Cell proliferation (MTT) assay**

26   To assess cell proliferation, N2a cells transfected with pcDNA3.1-*WH1(Δ/WT/A31V/ΔN37)-mCherry*, as

27   described above, were seeded 24 h after transfection into 96-well culture plates at a density of $6x10^4$

28   cells/well. The next day, MTT (thiazolyl blue tetrazolium bromide, Sigma; 0.5 mg/ml in PBS) was

1   supplied and, after 4 h of incubation at 37ºC, MTT was removed and replaced with 200 µl of DMSO.

2   Absorbance was measured at 570 nm in a Varioskan Flash plate reader (Thermo Fisher Scientific).

3   Absorbance values were normalized to those obtained in DMSO.

4   **Confocal microscopy**

5   Cells were directly observed at RT by confocal laser microscopy using a Leica TCS-SP5 microscope

6   with a 63x (NA = 1.4–0.60/Oil HCX PL APO) immersion objective. Laser lines used for excitation

7   were 514 nm (mCherry), 488 nm (Alexa 488 and Tag GFP2) and 405 nm (DAPI and ThS). Images were

8   acquired every 1 µm (Z-sections). Cells were fixed with 4% PFA in PBS for 15 min, rinsed three times

9   in PBS and nuclei staining, when required, was performed with 1 µg/ml DAPI solution (Merck-

10   Millipore) in PBS for 10 min, then rinsed three times with PBS. Coverslips were mounted with

11   Fluoromount-G medium (SouthernBiotech) on microscopic slides (Linealab). For amyloid

12   characterization of intracellular particles, transiently transfected N2a cells were grown on coverslips

13   coated with poly-L-lysine for 48 h. Cells were fixed with 4% PFA in PBS for 20 min and rinsed as

14   above. Then, cells were permeabilized with cold 50% methanol (Emsure) in Milli-Q H_2O for 5 min,

15   incubated with 0.05% thioflavin-S (ThS, Sigma) in 12.5% ethanol for 30 min and rinsed three times in

16   50% ethanol in destilled H_2O. Cells were then hydrated for 5 min in PBS and mounted.

17   **Statistical analysis**

18   All experiments were carried out in triplicate. GraphPath PRISM (v.6) software was used to estimate the

19   media and standard deviation of data points, and for the analysis of their statistical significance, either

20   through the Student´s *t*-test or one-way ANOVA.

21

22   **Proteomics**

23   **LC-MS analysis**

24   The following cell types were studied: i) N2a cells transfected with pcDNA3.1-*WH1(WT)-mCherry* or

25   pcDNA3.1-*mCherry*, and incubated with *in vitro*-assembled WH1(A31V) fibres for 48 h; ii) THN-

26   rtTA/SH-SY5Y cells having integrated pTRE3G-*WH1(WT)-TagGFP2* or pTRE3G-*TagGFP2*, both

27   after induction with Dox (0.5 µg/ml) for 48 h; and iii) naïve N2a and THN-rtTA/SH-SY5Y control cells

28   co-cultivated as in (i) and (ii). Whole cell extracts (see above) were partially resolved by SDS-PAGE

1   gel (10% polyacrylamide), so that the whole proteome became concentrated in the stacking/resolving

2   gel interface. The unresolved protein bands were visualized by Colloidal Blue Staining (Invitrogen),

3   excised into pieces (1 x 1 mm), and placed in 0.5 ml tubes and subjected to manual tryptic digestion

4   (Cristobo et al., 2001). The eluted tryptic peptides were dried by speed-vacuum centrifugation and then

5   desalted through ZipTip C18 Pipette tips (Millipore/Sigma-Aldrich). Samples were reconstituted in 10

6   μL of 0.1% formic acid before their analysis by nLC–MS/MS. All peptide separations were carried out

7   on an Easy-nLC 1000 nanosystem (Thermo Fisher Scientific). For each analysis, the sample was loaded

8   into an Acclaim PepMap 100 precolumn (Thermo Fisher Scientific) and eluted through a RSLC

9   PepMap C18 column (50 cm long, 75 μm inner diameter and 2 μm particle size; Thermo Scientific).

10   The mobile phase was 0.1% formic acid in water (solvent A) and 0.1% formic acid in acetonitrile

11   (solvent B). The gradient profile was set, at a flow rate of 300 nL/min, as follows: 5–35% solvent B for

12   100 min, 35%-45% solvent B for 20 min, 45%-100% solvent B for 5 min, and 100% solvent B for 15

13   min. Four microliters of each sample were injected. MS analysis was performed using a Q-Exactive

14   mass spectrometer (Thermo Scientific). Ionization was performed at 2,000 V of liquid junction voltage

15   and a capillary temperature of 270 °C. The full scan method comprised a m/z 300–1800 mass selection,

16   an Orbitrap resolution of 70,000 (at m/z 200), a target automatic gain control (AGC) value of $3x10^6$, and

17   100 ms of maximum injection time. After the survey scan, the 15 most intense precursor ions were

18   selected for MS/MS fragmentation. Fragmentation was performed with a normalized collision energy of

19   27 and MS/MS scans were acquired with a starting mass of m/z 200, $2x10^5$ AGC target, a resolution of

20   17,500 (at m/z 200), $8x10^3$ of intensity threshold, 2.0 m/z units as isolation window and 100 ms

21   maximum IT. Charge state screening was enabled to reject unassigned, singly charged and ≥ 7

22   protonated ions. A dynamic exclusion time of 30 s was used to discriminate against previously selected

23   ions.

24   **MS data analysis**

25   MS data were analyzed with Proteome Discoverer (version 1.4.1.14) (Thermo) using standardized

26   workflows. Mass spectra *.raw files were searched either against the *Mus musculus* SwissProt 2016

27   database (16,838 protein entries; for the N2a recipient cells), or the *Homo sapiens* SwissProt 2016

28   database (20,131 protein entries; for the SH-SY5Y recipient cells), using the Mascot search engine

1   (v.2.6, Matrix Science). In the latter case, limiting the survey to the human proteome excluded proteins

2   potentially coming from the donor murine cells. Precursor and fragment mass tolerance were set to 10

3   ppm and 0.02 Da, respectively, allowing 2 missed cleavages, carbamido methylation of cysteines as a

4   fixed modification, and methionine oxidation and acetylation N-terminal as a variable modification.

5   Identified peptides were filtered using Percolator algorithm with a q-value threshold of 0.01 (High

6   Confidence Filter settings, FDR < 1%) (Käll et al., 2007). Proteins contributing peptides detected at

7   least two times (PSM >1) or having more than one peptide identified were selected for further analysis.

8   Proteins identified in naïve N2a murine control cells when co-cultured with fibres were subtracted from

9   those found in N2a cells expressing WH1(WT)-mCherry or mCherry and also incubated with fibres.

10   Proteins found in naïve human THN-rtTA/SH-SY5Y control cells co-cultured with murine cells

11   donating WH1(A31V)-mCherry were subtracted from those in THN-rtTA/SH-SY5Ycells expressing

12   WH1(WT)-TagGFP2 or TagGFP2 and also co-cultured with the murine donor cells. A Boolean algebra

13   analysis (Venny, v.2.1; https://bioinfogp.cnb.csic.es/tools/venny/) was undertaken to identify those host

14   proteins found differentially under each experimental condition. The subset of proteins present in the

15   WH1(WT)-mCherry/TagGFP2 datasets solely upon incubation with the WH1(A31V) fibres/donor cells

16   were then classified according to functional gene ontology (GO) (GeneCards; Stelzer et al., 2010) and

17   cluster analysis (STRING v.11; Szklarczyk et al., 2019).

18

19   **References**

20   Aguzzi A, Falsig J. 2012. Prion propagation, toxicity and degradation. *Nature Neuroscience* **15**:936–

21   939. DOI: 10.1038/nn.3120.

22   Aguzzi A, Lakkaraju AKK. 2016. Cell Biology of Prions and Prionoids: A Status Report. *Trends in Cell*

23   *Biology* **26**:40–51. DOI: 10.1016/j.tcb.2015.08.007.

24   Chiti F, Dobson CM. 2017. Protein Misfolding, Amyloid Formation, and Human Disease: A Summary

25   of Progress Over the Last Decade. *Annual Review of Biochemistry* **86**:27–68. DOI: 10.1146/annurev-

26   biochem-061516-045115.

23

Clavaguera F, Bolmont T, Crowther RA, Abramowski D, Frank S, Probst A, Fraser G, Stalder AK, Beibel M, Staufenbiel M, Jucker M, Goedert M, Tolnay M. 2009. Transmission and spreading of tauopathy in transgenic mouse brain. *Nature Cell Biology* **11**:909–913. DOI: 10.1038/ncb1901.

Cristobo I, Larriba MJ, de los Ríos V, García F, Muñoz A, Casal JI. 2011. Proteomic analysis of 1α,25-dihydroxyvitamin D3 action on human colon cancer cells reveals a link to splicing regulation. *J Proteomics* **75**:384–397. DOI: 10.1016/j.jprot.2011.08.003.

de Villiers EM, Gunst K, Chakraborty D, Ernst C, Bund T, Zur Hausen H. 2019. A specific class of infectious agents isolated from bovine serum and dairy products and peritumoral colon cancer tissue. *Emerging Microbes & Infections* **8**:1205–1218. DOI: 10.1080/22221751.2019.1651620.

Diederix RE, Dávila C, Giraldo R, Lillo MP. 2008. Fluorescence studies of the replication initiator protein RepA in complex with operator and iteron sequences and free in solution. *FEBS Journal* **275**:5393–5407. DOI: 10.1111/j.1742-4658.2008.06669.x.

Duernberger Y, Liu S, Riemschoss K, Paulsen L, Bester R, Kuhn PH, Schölling M, Lichtenthaler SF, Vorberg I. 2018. Prion replication in the mammalian cytosol: Functional regions within a prion domain driving induction, propagation, and inheritance. *Molecular and Cellular Biology* **38**:e00111-18. DOI: 10.1128/MCB.00111-18.

Eisele YS, Obermüller U, Heilbronner G, Baumann F, Kaeser SA, Wolburg H, Walker LC, Staufenbiel M, Heikenwalder M, Jucker M. 2010. Peripherally applied Abeta-containing inoculates induce cerebral beta-amyloidosis. *Science* **330**:980–982. DOI: 10.1126/science.1194516.

Eisenberg DS, Sawaya MR. 2017. Structural studies of amyloid proteins at the molecular level. *Annual Review of Biochemistry* **86**:69–95. DOI: 0.1146/annurev-biochem-061516-045104.

Fernández C, Giraldo R. 2018. Modulation of the aggregation of the prion-like protein RepA-WH1 by chaperones in a cell-free expression system and in cytomimetic lipid vesicles. *ACS Synthetic Biology* **7**:2087–2093. DOI: 10.1021/acssynbio.8b00283.

Fernández C, González-Rubio G, Langer J, Tardajos G, Liz-Marzán LM, Giraldo R, Guerrero-Martínez A. 2016a. Nucleation of amyloid oligomers by RepA-WH1 prionoid-functionalized gold nanorods. *Angewandte Chemie International Edition* **55**:11237–11241. DOI: 10.1002/anie.201604970.

Fernández C, Núñez-Ramírez R, Jiménez M, Rivas G, Giraldo R. 2016b. RepA-WH1, the agent of an amyloid proteinopathy in bacteria, builds oligomeric pores through lipid vesicles. *Scientific Reports* **6**:23144. DOI: 10.1038/srep23144.

Fernández-Tresguerres ME, Moreno-Díaz de la Espina S, Gasset-Rosa F, Giraldo R. 2010. A DNA-promoted amyloid proteinopathy in *Escherichia coli. Molecular Microbiology* **77**:1456–1469. DOI: 10.1111/j.1365-2958.2010.07299.x.

Frederick KK, Debelouchina GT, Kayatekin C, Dorminy T, Jacavone AC, Griffin RG, Lindquist S. 2014. Distinct prion strains are defined by amyloid core structure and chaperone binding site dynamics. Chemistry & *Biology* **21**:295–305. DOI: 10.1016/j.chembiol.2013.12.013.

Friedland RP, Chapman MR. 2017. The role of microbial amyloid in neurodegeneration. *PLoS Pathogens* **13**:e1006654. DOI 10.1371/journal.ppat.1006654.

Frost B, Jacks RL, Diamond MI. 2009. Propagation of tau misfolding from the outside to the inside of a cell. *Journal of Biological Chemistry* **284**:12845–12852. DOI: 10.1074/jbc.M808759200.

Garrity SJ, Sivanathan V, Dong J, Lindquist S, Hochschild A. 2010. Conversion of a yeast prion protein to an infectious form in bacteria. *Proceedings of the National Academy of Sciences of the United States of America* **107**:10596–10601. DOI: 10.1073/pnas.0913280107.

Gasset-Rosa F, Coquel AS, Moreno-del Álamo M, Chen P, Song X, Serrano AM, Moreno-Díaz de la Espina S, Lindner AB, Giraldo R. 2014. Direct assessment in bacteria of prionoid propagation and phenotype selection by Hsp70 chaperone. *Molecular Microbiology* **91**:1070–1087. DOI: 10.1111/mmi.12518.

Gasset-Rosa F, Giraldo R. 2015. Engineered bacterial hydrophobic oligopeptide repeats in a synthetic yeast prion, [*REP-PSI*$^+$]. *Frontiers in Microbiology* **6**:311. DOI: 10.3389/fmicb.2015.00311.

Giraldo R, Fernández-Tornero C, Evans PR, Díaz-Orejas R, Romero A. 2003. A conformational switch between transcriptional repression and replication initiation in the RepA dimerization domain. *Nature Structural Biology* **10**:565–571. DOI: 10.1038/nsb937.

Giraldo R. 2007. Defined DNA sequences promote the assembly of a bacterial protein into distinct amyloid nanostructures. *Proceedings of the National Academy of Sciences of the United States of America* **104**:17388–17393. DOI: 10.1073/pnas.0702006104.

25

1   Giraldo R. 2019. Optogenetic navigation of routes leading to protein amyloidogenesis in bacteria.

2   *Journal of Molecular Biology* **431**:1186–1202. DOI: 10.1016/j.jmb.2019.01.037.

3   Goedert M. 2015. Alzheimer's and Parkinson's diseases: The prion concept in relation to assembled Aβ,

4   tau, and α-synuclein. *Science* **349**:1255555. DOI: 10.1126/science.1255555.

5   Goedert M, Eisenberg DS, Crowther RA. 2017. Propagation of Tau Aggregates and Neurodegeneration.

6   *Annual Review of Neuroscience* **40**:189–210. DOI: 10.1146/annurev-neuro-072116-031153.

7   Haelterman NA, Yoon WH, Sandoval H, Jaiswal M, Shulman JM, Bellen HJ. 2014. A mitocentric view

8   of Parkinson's disease. *Annual Review Neuroscience* **37**:137–159. doi: 10.1146/annurev-neuro-

9   071013-014317.

10 Hofmann JP, Denner P, Nussbaum-Krammer C, Kuhn PH, Suhre MH, Scheibel T, Lichtenthaler SF,

11   Schätzl HM, Bano D, Vorberg IM. 2013. Cell-to-cell propagation of infectious cytosolic protein

12   aggregates. *Proceedings of the National Academy of Sciences of the United States of America*

13   **110**:5951–5956. DOI: 10.1073/pnas.1217321110.

14 Hosp F, Vossfeldt H, Heinig M, Vasiljevic D, Arumughan A, Wyler E, GERAD1 Consortium,

15   Landthaler M, Hubner N, Wanker EE, Lannfelt L, Ingelsson M, Lalowski M, Voigt A, Selbach M.

16   2015. Quantitative interaction proteomics of neurodegenerative disease proteins. *Cell Reports*

17   **11**:1134–1146. DOI: 10.1016/j.celrep.2015.04.030.

18 Hwang D, Lee IY, Yoo H, Gehlenborg N, Cho JH, Petritis B, Baxter D, Pitstick R, Young R, Spicer D,

19   Price ND, Hohmann JG, Dearmond SJ, Carlson GA, Hood LE. 2009. A systems approach to prion

20   disease. Molecular Systems Biology 5:252. DOI: 10.1038/msb.2009.10.

21 Jucker M, Walker LC. 2018. Propagation and spread of pathogenic protein assemblies in

22   neurodegenerative diseases. *Nature Neuroscience* **21**:1341–1349. DOI: 10.1038/s41593-018-0238-6.

23 Käll L, Canterbury JD, Weston J, Noble WS, MacCoss MJ. 2007. Semi-supervised learning for peptide

24   identification from shotgun proteomics datasets. *Nature Methods* 4:923–925. DOI:

25   10.1038/nmeth1113.

26 Kfoury N, Holmes BB, Jiang H, Holtzman DM, Diamond MI. 2012. Trans-cellular propagation of Tau

27   aggregation by fibrillar species. *Journal of Biological Chemistry* **287**:19440–19451. DOI:

28   10.1074/jbc.M112.346072.

Kilic T, Popov AN, Burk-Körner A, Koromyslova A, Zur Hausen H, Bund T, Hansman GS. 2019. Structural analysis of a replication protein encoded by a plasmid isolated from a multiple sclerosis patient. *Acta Crystallographica D* **75**:498–504. DOI: 10.1107/S2059798319003991.

Kim YE, Hosp F, Frottin F, Ge H, Mann M, Hayer-Hartl M, Hartl FU. 2016. Soluble Oligomers of PolyQ-Expanded Huntingtin Target a Multiplicity of Key Cellular Factors. *Molecular Cell* **63**:951-964. DOI: 10.1016/j.molcel.2016.07.022.

Kordower JH, Chu Y, Hauser RA, Freeman TB, Olanow CW. 2008. Lewy body-like pathology in long-term embryonic nigral transplants in Parkinson's disease. *Nature Medicine* **14**:504–506. DOI: 10.1038/nm1747.

Krammer C, Kryndushkin D, Suhre MH, Kremmer E, Hofmann A, Pfeifer A, Scheibel T, Wickner RB, Schätzl HM, Vorberg I. 2009. The yeast Sup35NM domain propagates as a prion in mammalian cells. *Proceedings of the National Academy of Sciences of the United States of America* **106**:462–467. DOI: 10.1073/pnas.0811571106.

Liu S, Hossinger A, Hofmann JP, Denner P, Vorberg IM. 2016. Horizontal transmission of cytosolic Sup35 prions by extracellular vesicles. 2016. *mBio* **7**:e00915-16. DOI: 10.1128/mBio.00915-16.

Lu JX, Qiang W, Yau WM, Schwieters CD, Meredith SC, Tycko R. 2013. Molecular structure of β-amyloid fibrils in Alzheimer's disease brain tissue. *Cell* **154**:1257–1268. DOI: 10.1016/j.cell.2013.08.035.

Luk KC, Kehm VM, Zhang B, O'Brien P, Trojanowski JQ, Lee VM. 2012. Intracerebral inoculation of pathological α-synuclein initiates a rapidly progressive neurodegenerative α-synucleinopathy in mice. *Journal of Experimental Medicine* **209**:975–986. DOI: 10.1084/jem.20112457.

Luk KC, Song C, O'Brien P, Stieber A, Branch JR, Brunden KR, Trojanowski JQ, Lee VM. 2009. Exogenous alpha-synuclein fibrils seed the formation of Lewy body-like intracellular inclusions in cultured cells. *Proceedings of the National Academy of Sciences of the United States of America* **106**:20051–20056. DOI: 10.1073/pnas.0908005106.

Markmiller S, Soltanieh S, Server KL, Mak R, Jin W, Fang MY, Luo EC, Krach F, Yang D, Sen A, Fulzele A, Wozniak JM, Gonzalez DJ, Kankel MW, Gao FB, Bennett EJ, Lécuyer E, Yeo GW.

2018. Context-Dependent and Disease-Specific Diversity in Protein Interactions within Stress Granules. *Cell* **172**:590–604. DOI: 10.1016/j.cell.2017.12.032.

Mathys H, Davila-Velderrain J, Peng Z, Gao F, Mohammadi S, Young JZ, Menon M, He L, Abdurrob F, Jiang X, Martorell AJ, Ransohoff RM, Hafler BP, Bennett DA, Kellis M, Tsai LH. 2019. Single-cell transcriptomic analysis of Alzheimer's disease. *Nature* **570**:332–337. DOI: 10.1038/s41586-019-1195-2.

Molina-García L, Gasset-Rosa F, Moreno-del Álamo M, Fernández-Tresguerres ME, Moreno-Díaz de la Espina S, Lurz R, Giraldo R. 2016. Functional amyloids as inhibitors of plasmid DNA replication. *Scientific Reports* **6**:25425. DOI: 10.1038/srep25425.

Molina-García L, Giraldo R. 2014. Aggregation interplay between variants of the RepA-WH1 prionoid in *Escherichia coli*. *Journal of Bacteriology* **196**:2536–2542. DOI: 10.1128/JB.01527-14.

Molina-García L, Moreno-del Álamo M, Botias P, Martín-Moldes Z, Fernández M, Sánchez-Gorostiaga A, Alonso-del Valle A, Nogales J, García-Cantalejo J, Giraldo R. 2017. Outlining core pathways of amyloid toxicity in bacteria with the RepA-WH1 prionoid. *Frontiers in Microbiology* **8**:539. DOI: 10.3389/fmicb.2017.00539.

Moreno-del Álamo M, Moreno-Díaz de la Espina S, Fernández-Tresguerres ME, Giraldo R. 2015. Pre-amyloid oligomers of the proteotoxic RepA-WH1 prionoid assemble at the bacterial nucleoid. *Scientific Reports* **5**:14669. DOI: 10.1038/srep14669.

Norambuena A, Wallrabe H, Cao R, Wang DB, Silva A, Svindrych Z, Periasamy A, Hu S, Tanzi RE, Kim DY, Bloom GS. 2018. A novel lysosome-to-mitochondria signaling pathway disrupted by amyloid-β oligomers. *EMBO Journal* **37**:e100241. DOI: 10.15252/embj.2018100241.

Olzscha H, Schermann SM, Woerner AC, Pinkert S, Hecht MH, Tartaglia GG, Vendruscolo M, Hayer-Hartl M, Hartl FU, Vabulas RM. 2011. Amyloid-like aggregates sequester numerous metastable proteins with essential cellular functions. *Cell* **144**:67–78. DOI: 10.1016/j.cell.2010.11.050.

Perov S, Lidor O, Salinas N, Golan N, Tayeb-Fligelman E, Deshmukh M, Willbold D, Landau M. 2019. Structural Insights into Curli CsgA Cross-β Fibril Architecture Inspire Repurposing of Anti-amyloid Compounds as Anti-biofilm Agents. *PLoS Pathogens* **15**:e1007978. DOI: 10.1371/journal.ppat.1007978.

1   Polymenidou M, Cleveland DW. 2012. Prion-like spread of protein aggregates in neurodegeneration.

2   *Journal of Experimental Medicine* **209**:889–893. DOI: 10.1084/jem.20120741.

3   Prusiner SB. 1998. Prions. *Proceedings of the National Academy of Sciences of the United States of*

4   *America* **95**:13363–13383.

5   Prusiner SB. 2013. Biology and genetics of prions causing neurodegeneration. *Annual Review of*

6   *Genetics* **47**:601-623. DOI: 10.1146/annurev-genet-110711-155524.

7   Prusiner SB, Woerman AL, Mordes DA, Watts JC, Rampersaud R, Berry DB, Patel S, Oehler A, Lowe

8   JK, Kravitz SN, Geschwind DH, Glidden DV, Halliday GM, Middleton LT, Gentleman SM,

9   Grinberg LT, Giles K. 2015. Evidence for α-synuclein prions causing multiple system atrophy in

10   humans with parkinsonism. *Proceedings of the National Academy of Sciences of the United States of*

11   *America* **112**:E5308–E5317. DOI: 10.1073/pnas.1514475112.

12   Qiang W, Yau WM, Lu JX, Collinge J, Tycko R. 2017. Structural variation in amyloid-β fibrils from

13   Alzheimer's disease clinical subtypes. *Nature* **541**:217–221. DOI: 10.1038/nature20814.

14   Riemschoss K, Arndt V, Bolognesi B, von Eisenhart-Rothe P, Liu S, Buravlova O, Duernberger Y,

15   Paulsen L, Hornberger A, Hossinger A, Lorenzo-Gotor N, Hogl S, Müller SA, Tartaglia G,

16   Lichtenthaler SF, Vorberg IM. 2019. Fibril-induced glutamine-/asparagine-rich prions recruit stress

17   granule proteins in mammalian cells. *Life Science Alliance* **2**:e201800280. DOI:

18   10.26508/lsa.201800280.

19   Seyfried NT, Dammer EB, Swarup V, Nandakumar D, Duong DM, Yin L, Deng Q, Nguyen T, Hales

20   CM, Wingo T, Glass J, Gearing M, Thambisetty M, Troncoso JC, Geschwind DH, Lah JJ, Levey AI.

21   2017. A Multi-network Approach Identifies Protein-Specific Co-expression in Asymptomatic and

22   Symptomatic Alzheimer's Disease. *Cell Systems* **4**:60–72. DOI: 10.1016/j.cels.2016.11.006.

23   Scheckel C, Aguzzi A. 2018. Prions, prionoids and protein misfolding disorders. *Nature Reviews in*

24   *Genetics* **19**:405–418. DOI: 10.1038/s41576-018-0011-4.

25   Sonati T, Reimann RR, Falsig J, Baral PK, O'Connor T, Hornemann S, Yaganoglu S, Li B, Herrmann

26   US, Wieland B, Swayampakula M, Rahman MH, Das D, Kav N, Riek R, Liberski PP, James MN,

27   Aguzzi A. 2013. The toxicity of antiprion antibodies is mediated by the flexible tail of the prion

28   protein. *Nature* **501**:102–106. DOI: 10.1038/nature12402.

1   Soto C. 2012. Transmissible proteins: expanding the prion heresy. *Cell* **149**:968–977. DOI:

2   10.1016/j.cell.2012.05.007.

3   Stöhr J, Watts JC, Mensinger ZL, Oehler A, Grillo SK, DeArmond SJ, Prusiner SB, Giles K. 2012.

4   Purified and synthetic Alzheimer's amyloid beta (Aβ) prions. *Proceedings of the National Academy*

5   *of Sciences of the United States of America* **109**:11025–11030. DOI: 10.1073/pnas.1206555109.

6   Stelzer G, Rosen R, Plaschkes I, Zimmerman S, Twik M, Fishilevich S, Iny Stein T, Nudel R, Lieder I,

7   Mazor Y, Kaplan S, Dahary D, Warshawsky D, Guan-Golan Y, Kohn A, Rappaport N, Safran M,

8   Lancet D. 2020. The GeneCards Suite: From Gene Data Mining to Disease Genome Sequence

9   Analysis. *Current Protocols in Bioinformatics* **54**:1.30.1–1.30.33. DOI: 10.1002/cpbi.5.

10   Szklarczyk D, Gable AL, Lyon D, Junge A, Wyder S, Huerta-Cepas J, Simonovic M, Doncheva NT,

11   Morris JH, Bork P, Jensen LJ, Mering CV. 2019. STRING v11: protein-protein association networks

12   with increased coverage, supporting functional discovery in genome-wide experimental datasets.

13   *Nucleic Acids Research* **47**:D607–D613. DOI: 10.1093/nar/gky1131.

14   Torreira E, Moreno-del Álamo M, Fuentes-Perez ME, Fernández C, Martín-Benito J, Moreno-Herrero

15   F, Giraldo R, Llorca O. 2015. Amyloidogenesis of bacterial prionoid RepA-WH1 recapitulates dimer

16   to monomer transitions of RepA in DNA replication initiation. *Structure* **23**:183–189. DOI:

17   10.1016/j.str.2014.11.007.

18   Wang P, Deng J, Dong J, Liu J, Bigio EH, Mesulam M, Wang T, Sun L, Wang L, Lee AY, McGee WA,

19   Chen X, Fushimi K, Zhu L, Wu JY. 2019. TDP-43 induces mitochondrial damage and activates the

20   mitochondrial unfolded protein response. *PLoS Genetics* **15**:e1007947. DOI:

21   10.1371/journal.pgen.1007947.

22   Watts JC, Condello C, Stöhr J, Oehler A, Lee J, DeArmond SJ, Lannfelt L, Ingelsson M, Giles K,

23   Prusiner SB. 2014. Serial propagation of distinct strains of Aβ prions from Alzheimer's disease

24   patients. *Proceedings of the National Academy of Sciences of the United States of America*

25   **111**:10323–10328. DOI: 10.1073/pnas.1408900111.

26   Wickner RB, Shewmaker FP, Bateman DA, Edskes HK, Gorkovskiy A, Dayani Y, Bezsonov EE. 2015.

27   Yeast prions: structure, biology, and prion-handling systems. *Microbiology and Molecular Biology*

28   *Reviews* **79**:1–17. DOI: 10.1128/MMBR.00041-14.

1   Woerner AC, Frottin F, Hornburg D, Feng LR, Meissner F, Patra M, Tatzelt J, Mann M, Winklhofer

2   KF, Hartl FU, Hipp MS. 2016. Cytoplasmic protein aggregates interfere with nucleocytoplasmic

3   transport of protein and RNA. *Science* **351**:173–176. DOI: 10.1126/science.aad2033.

4   Yuan AH, Hochschild A. 2017. A bacterial global regulator forms a prion. *Science* **355**:198–201. DOI:

5   10.1126/science.aai7776.

6

Acknowledgements

16

Author contributions

18   ARG carried out most experimental work and analysed data; CF prepared the fluorescence-labelled

19   fibres and helped with their transfection and data analysis; MMdA made the plasmid constructs and

20   earlier work with the SH-SY5Y cells; VdlR performed the proteomic analyses; IMV hosted ARG and

21   provided expertise on the cell biology of cytoplasmic propagation of prion-like proteins; RG conceived

22   the project, analysed data and wrote the manuscript with contributions from all the authors.

23

Conflict of interest

25   The authors declare that they have no conflict of interest.

26

Figure legends

31

1   **Fig. 1.** Expression of WH1(A31V)-mCherry in the cytosol of murine N2a cells.

2   (**A**) Confocal maximum-intensity projection images of N2a cells expressing WH1(WT/A31V/ΔN37)-

3   mCherry, or mCherry as a control, 48 h after being transiently transfected (red). White arrows mark the

4   small WH1(A31V)-mCherry fluorescent foci, whereas the large WH1(ΔN37)-mCherry inclusions are

5   indicated with asterisks. Nuclei were stained with DAPI (blue). Yellow arrow points to an altered

6   nucleus.

7   (**B**) Quantitative analysis of condensed/fragmented nuclei in N2a transfected cells that expressed for 24,

8   48 and 72 h either WH1(WT/A31V/ΔN37)-mCherry or the mCherry control. The total number of cells

9   of each type expressing the mCherry fluorescence is displayed below the X-axis.

10   (**C**) N2a cell viability, quantitatively estimated from a MTT reduction assay, in response to transient

11   expression of the RepA-WH1 variants for 24, 48 and 72 h. The inferred cytotoxicity of the proteins

12   expressed was: WH1(A31V) >> WH1(ΔN37) > WH1(WT) > mCherry.

13   In (B) and (C), bars correspond to the mean values from three independent transfections (n = 3). One-

14   way ANOVA test was performed (*, $p < 0.1$; **, $p < 0.01$; ***, $p < 0.001$; ****, $p < 0.0001$; ns: not

15   significant).

16

17   **Fig. 2.** The particles assembled by WH1(A31V)-mCherry at the cytosol of murine N2a cells are

18   amyloids.

19   Confocal maximum-intensity projection images of N2a cells transiently expressing for 48 h

20   WH1(WT/A31V/ΔN37)-mCherry, or mCherry as control (red). Cells were stained with ThS (blue) for

21   amyloid detection. Arrows mark examples of the intracellular WH1(A31V)-mCherry puncta, whereas

22   some of the ThS-positive foci are indicated with asterisks. Just the WH1(A31V)-mCherry particles are

23   amyloid by nature.

24

25   **Fig. 3.** Uptake of *in vitro*-assembled, Alexa 488-labelled WH1(A31V) amyloid fibres by murine N2a

26   cells results in the formation of foci by endogenous WH1(WT)-mCherry.

27   (**A**) Experimental setup to study the induction of endogenous WH1(WT)-mCherry foci upon the uptake

28   of exogenous WH1(A31V) fibres. N2a cells were transiently transfected with plasmids expressing

32

1 WH1(WT)-mCherry or the mCherry control (1) and immediately incubated with *in vitro*-assembled

2 WH1(A31V) fibrils (2) for 24, 48 and 72 h.

3 (**B**) Confocal section images of the experiment outlined in (A) (48 h after fibre addition, unfixed cells).

4 Exogenous WH1(A31V) fibres (green) were taken up by N2a cells expressing (red) either mCherry

5 (top), or WH1(WT)-mCherry (bottom). The generated intracellular WH1(WT)-mCherry amyloid foci

6 are indicated by arrows.

7 (**C**) Percentage of mCherry or WH1(WT)-mCherry expressing N2a cells bearing fluorescent foci 48 h

8 after incubation with WH1(A31V) fibres. Bars in the graph display the means from three independent

9 experiments (n = 3). The total number of cells of each type counted is displayed below the X-axis. For

10 statistical analysis, Student's *t*-test was performed (***, $p < 0.001$; ****, $p < 0.0001$).

11

12 **Fig. 4.** The particles induced by transfected WH1(A31V) fibres on WH1(WT)-mCherry at the cytosol of

13 murine N2a cells are amyloidogenic.

14 Confocal maximum-intensity projections of N2a cells expressing soluble mCherry or WH1(WT)-

15 mCherry (red), incubated for 48 h with *in vitro*-assembled, Alexa 488-labelled WH1(A31V) fibres

16 (green). Cells were then stained with ThS (blue) for amyloid detection. Three of the fibre-nucleated

17 WH1(WT)-mCherry puncta (arrows) that were also positive for ThS (asterisks) are highlighted.

18

19 **Fig. 5.** Uptake by human SH-SY5Y cells of WH1(A31V)-mCherry generated by murine N2a cells

20 results in formation of foci by endogenously expressed WH1(WT)-TagGFP2.

21 (**A**) Experimental setup to study horizontal propagation of WH1(A31V) between cell lines. Twenty-four

22 h after being transfected with plasmids, donor N2a cells transiently expressing soluble WH1(WT)-

23 mCherry, or the amyloidogenic WH1(A31V)-mCherry, were co-cultured for up to 7 days with THN-

24 rtTA/SH-SY5Y receptor cells stably expressing, upon Dox induction, either WH1(WT)-TagGFP2 or

25 TagGFP2.

26 (**B**) *Left*: Confocal sections of cells in cultures as sketched in (A) in which the receptor cells (R) were

27 expressing the TagGFP2 control, while the donor cells (D) were either WH1(WT)-mCherry or

28 WH1(A31V)-mCherry. No large fluorescent puncta were observed after 5 days. DAPI staining of

33

1   nuclear DNA was carried out. *Right*: Percentage of THN-rtTA/SH-SY5Y/TagGFP2 receptor cells (R)

2   bearing intracellular foci after 5 days of co-culture with transiently transfected WH1(WT)-mCherry or

3   WH1(A31V)-mCherry N2a donors (D).

4   (**C**) *Left*: Confocal sections of cells in cultures as those in (B), but in which the receptors (R) were

5   expressing WH1(WT)-TagGFP2 instead of just TagGFP2. Bright green spots (arrows) were

6   differentially promoted by the cells donating WH1(A31V)-mCherry, but not by those expressing

7   WH1(WT)-mCherry. *Right*: Quantitative analysis of intercellular propagation of RepA-WH1.

8   Percentage of THN-rtTA/SH-SY5Y/WH1(WT)-TagGFP2 receptor cells (R) bearing intracellular foci

9   after 5 days of co-culture with transiently transfected WH1(WT)-mCherry or WH1(A31V)-mCherry

10   N2a donors (D).

11   Bars displayed in both histograms are the mean of three independent experiments (n = 3). The total

12   number of cells of each type counted is displayed below the X-axes. For statistical analysis, Student's *t*-

13   test was performed (***, $p < 0.001$; ns, not statistically significant).

14

15   **Fig. 6.** Proteome-wide responses of mammalian cells expressing WH1(WT) to either *in vitro* assembled

16   WH1(A31V) fibres or WH1(A31V)-mCherry released from co-cultured cells.

17   The cartoon displays, overlaid to the sketch of a mammalian cell, the names of the proteins

18   differentially and uniquely found in cells expressing WH1(WT)-mCherry, and on which amyloids were

19   templated by either fibre-to-cell or cell-to-cell transmission. Proteins are grouped in boxes according to

20   their subcellular location, with numbers representing the fraction of the proteome dataset allocated to

21   each compartment. Colour coding refers to the main function reported in the literature for these proteins

22   (see the legend below, including the fraction of the proteins placed in each functional group).

23

24   ## Supplementary Files

25   **Fig. S1.** Transient expression in mammalian cell lines of distinct variants of the bacterial prion-like

26   protein RepA-WH1 fused to the red fluorescent protein mCherry.

27   (**A**) Schematic linear representation of the pcDNA3.1 plasmid constructs used to transiently express

28   either the distinct WH1-mCherry fusions or the mCherry control in mammalian cell lines.

(**B**) Assessing the expression of the WH1-mCherry derived constructions (WT/A31V/ΔN37; ≈55 kDa), or the mCherry control (35 kDa), in (A) by Western-blotting of soluble lysates 48 h after transient transfection of N2a, SH-SY5Y and HeLa cell lines. Protein constructions were detected using an anti-mCherry antibody. Actin (42 kDa) as a loading control was visualized with an anti-actin antibody. The insoluble fraction (pellet) of cells expressing WH1(ΔN37) in the N2a cells is also shown, compatible with its tendency to form large foci in bacteria (Gasset-Rosa et al., 2014; Molina-García et al., 2014).

Fig. S2. *In vitro*-assembled and Alexa 488-labelled WH1(A31V) fibres used for co-cultivation with the murine N2a cells.

(**A**) Negative staining TEM micrographs of the fibres before (*left*) and after (*right*) being disrupted by means of sonication, previously to their addition to the transfected N2a cells.

(**B**) Confocal section of the fibre samples. Green fluorescence from the tracer Alexa 488-labelled WH1(A31V) molecules incorporated into the fibres is evident.

Fig. S3. Experimental setting used for the stable expression of proteins in the human neuroblastoma cell line SH-SY5Y.

(**A**) Tet-ON, doxycline (Dox)-dependent expression cascade from the integrated pCMV-Tet3G transactivator (rtTA; *left*) and the pTRE3G response plasmids (*right*).

(**B**) Western-blots of protein extracts from THN-rtTA/SH-SY5Y cells expressing WH1(WT)-TagGFP2 or TagGFP2 upon induction for 48 h with 0.5 µg/ml Dox. Protein fusions were probed with an anti-GFP antibody, whereas detection of vinculin (≈123 kDa) was used as a loading control.

(**C**) Flow cytometry histograms (FL1 channel) highlighting the population of live THN-rtTA/SH-SY5Y cells expressing (green) or not (grey) the engineered fluorescent proteins after 48 h of culture in the presence of Dox (see B). Mean fluorescence intensity (MFI) TagGFP2: 3.44; MFI WH1(WT)-TagGFP2: 1.61.

(**D**) Confocal maximum-intensity projections images of THN-rtTA/SH-SY5Y clones stably expressing the rtTA transactivator and TagGFP2, or WH1(WT)-TagGFP2 (green), 48 h after Dox addition. Nuclei

1   were visualized using DAPI (blue). Both proteins are expressed soluble (diffuse fluorescence) in the

2   cytoplasm.

3

4   **Fig. S4.** Systems analysis of the response of murine N2a (**A**) and human THN-rtTA/SH-SY5Y (**B**) cells,

5   expressing soluble WH1(WT) or its fluorescent tags, to co-cultivation with the *in vitro*-assembled and

6   the cell-released WH1(A31V) amyloids, respectively. Venn diagrams (*top*) indicate the number of

7   proteins exclusively identified in the WH1(WT)-mCherry/TagGFP2 or in the control

8   mCherry/TagGFP2 cells (Figure 6), as well as in both of them, over those found in the naïve N2a or

9   THN-rtTA/SH-SY5Y backgrounds when challenged with the same fibres or donor cells, which were

10   subtracted. STRING v.11 (Szklarczyk et al., 2019) functional clustering analysis (*bottom*; inset:

11   program settings) was performed, using all available prediction sources, for the proteins identified as

12   differentially expressed under both experimental settings. After removing the unconnected nodes, the

13   remaining clusters, similar under both amyloid transmission scenarios, point to contributions of the

14   mitochondrial membrane respiratory complexes, protein quality control and signalling/trafficking to the

15   RepA-WH1 'generic' model of amyloidosis in mammalian cells.

16

17   **Supplemental Dataset S1.** ESI-MS/MS analysis of the proteome response of mouse N2a cells to

18   WH1(A31V) fibril uptake-promoted amyloidogenesis.

19

20   **Supplemental Dataset S2.** ESI-MS/MS analysis of the proteome response of human THN-rtTA/SH-

21   SY5Y cells on transmission of WH1(A31V)-mCherry from murine N2a cells.

22

23   **Table S1.** Subset of proteins in Datasets S1 and S2 matching proteins/genes differentially located in

24   published system analyses of aggregation-triggered neurodegeneration.
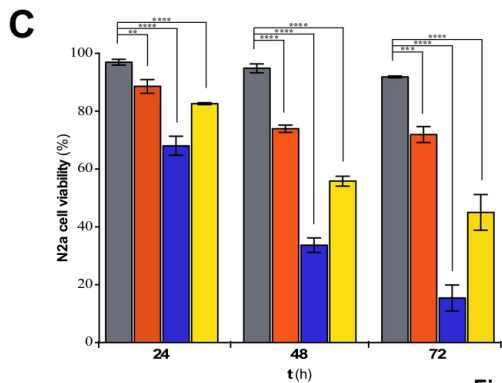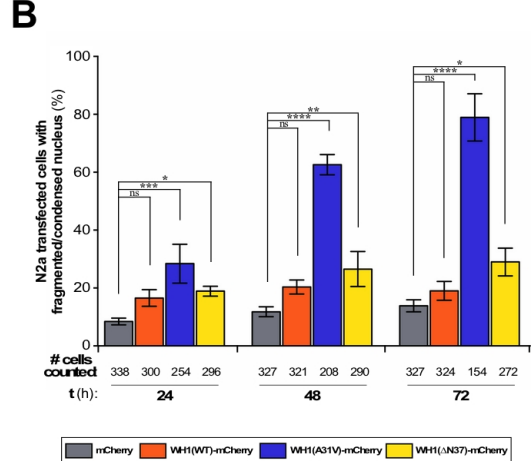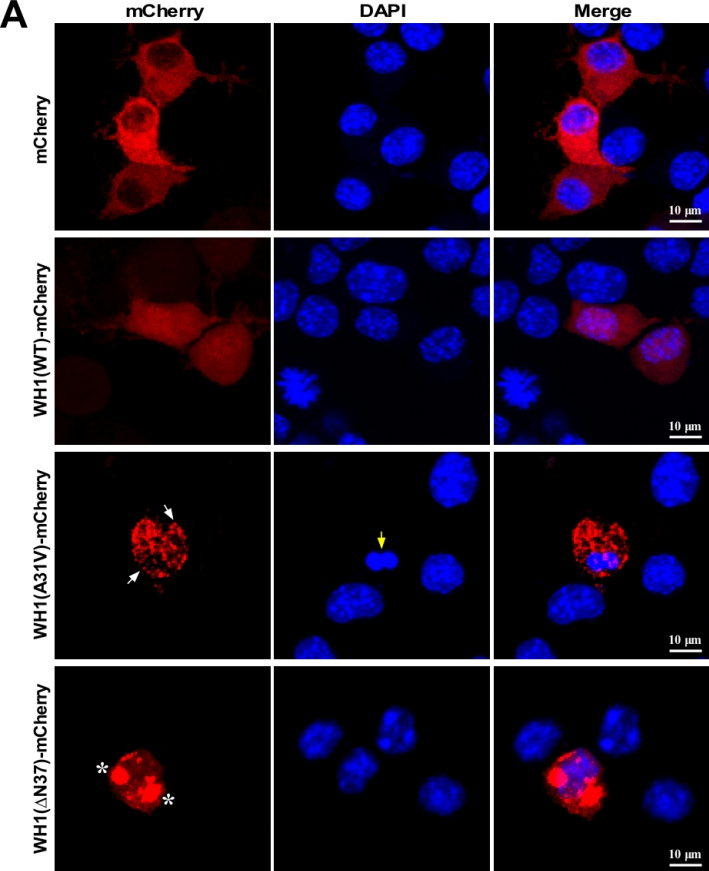
25

A

mCherry | DAPI | Merge

mCherry

WH1(WT)-mCherry

WH1(A31V)-mCherry

WH1(ΔN37)-mCherry

10 μm

B

N2a transfected cells with fragmented/condensed nucleus (%)

cells counted

338	300	254	296	327	321	208	290	327	324	154	272

t (h): 24 | 48 | 72

■ mCherry ■ WH1(WT)-mCherry ■ WH1(A31V)-mCherry ■ WH1(ΔN37)-mCherry

C

N2a cell viability (%)

t (h): 24 | 48 | 72

Fig. 1

Fig. 2

A

Uptake of **fibres** and **foci** induction

N2a cells

t = 24 h   t = 48 h   // t = 72 h

Confocal microscopy

1 Plasmid transfection
2 WH1(A31V) fibres addition

B

| mCherry | Alexa 488 | Merge |

mCherry + WH1(A31V) fibres

10 µm

WH1(WT) + WH1(A31V) fibres

10 µm

C

% Cells bearing foci / expressing cells

****
***

Fibrils: −   +   −   +
cells
counted: 298   315   311   324

mCherry   WH1(WT)-mCherry

Fig. 3

Fig. 4

A

N2a / pCDNA3.1 transient transfection
WH1(WT/A31V)-mCherry

t = 24 h

+ Dox

SH-SY5Y / THN-rtTA stable expression
WH1(WT)-TagGFP2

t = 24 h   over time up to 1 week

Donor   Receptor

Confocal microscopy

B

	GFP	DAPI	Merge
WT (D) / GFP (R)			10 µm
A31V (D) / GFP (R)			10 µm
WT (D) / WT (R)			10 µm
A31V (D) / WT (R)			10 µm

C

Receptor cells bearing foci (%)

ns

WT (D) / GFP (R)   A31V (D) / GFP (R)

\# cells counted: 445   473

Receptor cells bearing foci (%)

***

WT (D) / WT (R)   A31V (D) / WT (R)

\# cells counted: 440   320

Fig. 5

FIBRE-to-CELL

EMC7
EMC10
LPCAT3
P3H1
PEF1
PLD3
SEL1L
TAPBP
TBL2
TMED1

0.24

CELL-to-CELL

EPHX1   MLEC
EPM2AIP1   MYDGF
ERLEC1   PIGK
H6PD   PTPLAD1
HM13   RETSAT
IER3IP1   SEC61A1
JAGN1   SRPR
EMC1   STT3A
MIA3   STT3B

0.21

FIBRE-to-CELL

ADO
AMPD2
FBXO2
KRT2
MRI1
PLIN2

0.14

CELL-to-CELL

CHORDC1
DGKA
DNAJB4
GCA
GNPDA1
PSMD6
SEC24C

0.08

FIBRE-to-CELL

TMEM167A

0.02

CELL-to-CELL

ARFGAP2
COPB2
GOLT1B
OSBP
TPST1

0.06

FIBRE-to-CELL

DPP7
HEXB
TPP1

0.07

CELL-to-CELL

ARSA
FUCA1
GM2A
MAN2B1

0.05

FIBRE-to-CELL

RCC1
SAFB
SNRPG

0.07

CELL-to-CELL

CUL1
DDX21
DIS3
H2AFY
LEMD2
PRMT5
PRPF8
RABL3
STK4
TPP2
TRMT61A

0.13

FIBRE-to-CELL

CISD2
COQ3
COX6C
CRAT
MPC2
NDUFB8
SLC25A20
TMEM65
USMG5

0.21

CELL-to-CELL

APOOL   NDUFS6
BAK1   NDUFS7
COX5B   NNT
CPT1A   ROMO1
DNAJC11   SFXN2
HSDL1   SLC25A1
NDUFA11   SLC25A15
NDUFAB1   SPNS1
NDUFB5   TMEM14C
NDUFB7   TST

0.24

FIBRE-to-CELL

ABCB6
MCAM

0.05

CELL-to-CELL

AAMP
ATP6AP2
CD47
CLPTM1
CYP20A1
ITGA1
SLC44A2
SLC7A5
TM9SF3

0.11

FIBRE-to-CELL

TMEM165

0.02

CELL-to-CELL

FLOT1
WASHC4
ROBLD3

0.04

FIBRE-to-CELL

ECH1

0.02

CELL-to-CELL

CORO1B
EML4

0.02

Extracellular

FIBRE-to-CELL

CCDC134
CRTAP
F2
ISG15
NUCB2
TMEM256

0.14

CELL-to-CELL

CLEC3B
ITIH4
LUM
MFGE8
PCOLCE
PCYOX1L

0.07

Cytosol
ER
Golgi
Lysosome
Nucleus
Mitochondria
Endosome
Peroxisome
Plasma membrane
Cytoskeleton

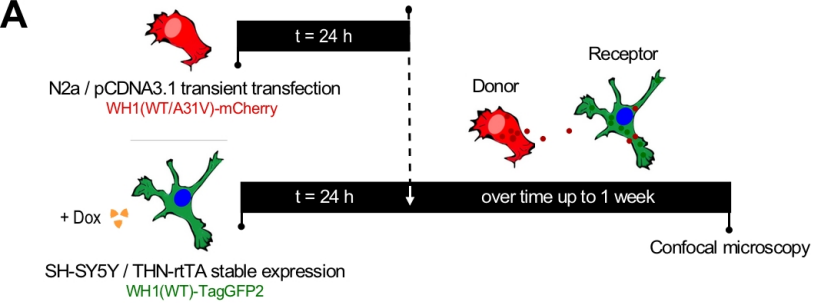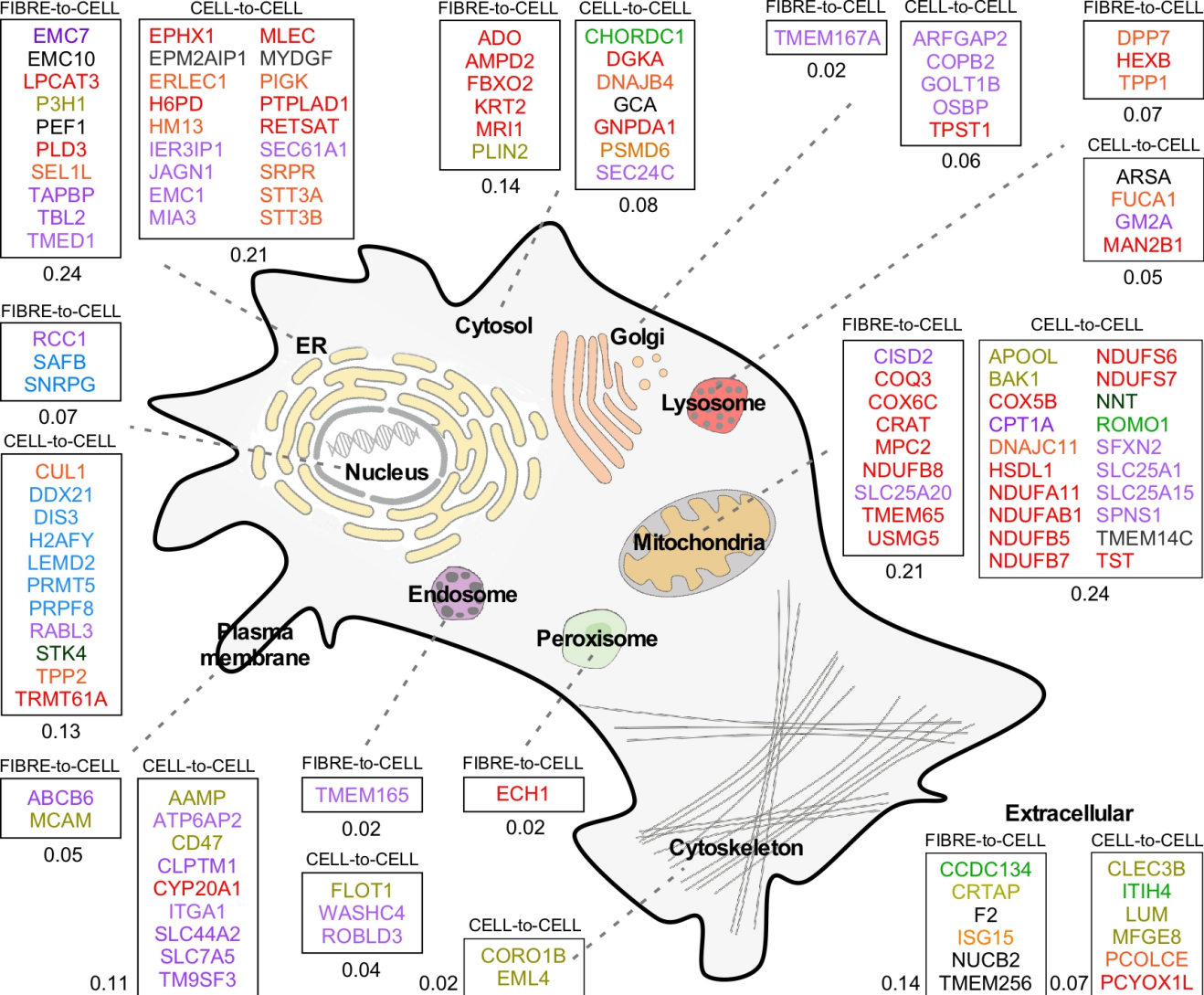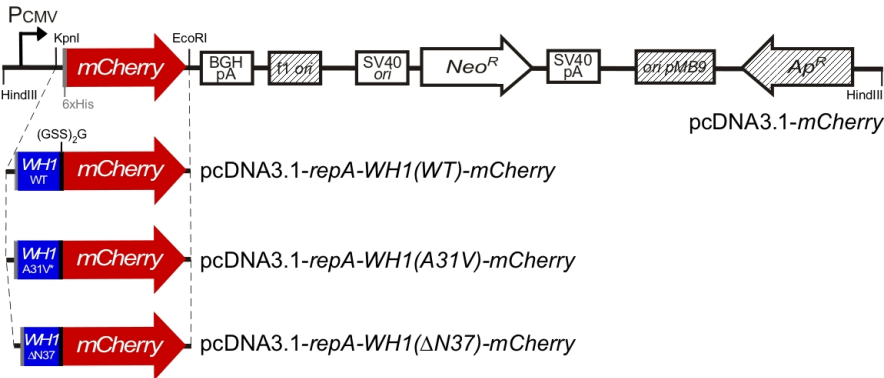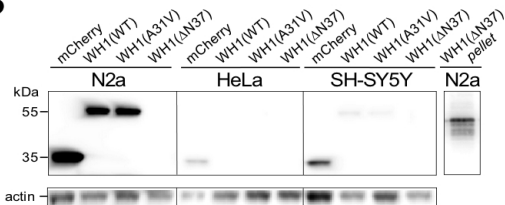|	FIBRE-to-CELL	CELL-to-CELL
Cellular structure: cytoskeleton and cellular adhesion	0.09	0.12
Gene expression and genome maintenance: transcription, replication, translation, repair, splicing, chromosomes	0.05	0.07
Metabolism	0.38	0.25
Protein quality control: chaperones, proteases, post-translational mod.	0.10	0.15
Signalling or transport: ER ⟶ Golgi ⟶ membrane	0.24	0.29
Stress or response to infection: autophagy, apoptosis	0.02	0.03
Others / Unknown function	0.12	0.08

Fig. 6

A

P_CMV

HindIII — KpnI — *mCherry* (6xHis) — EcoRI — BGH pA — f1 ori — SV40 ori — Neo^R — SV40 pA — ori pMB9 — Ap^R — HindIII

pcDNA3.1-*mCherry*

(GSS)₂G

WH1 WT — *mCherry* — pcDNA3.1-*repA-WH1(WT)-mCherry*

WH1 A31V* — *mCherry* — pcDNA3.1-*repA-WH1(A31V)-mCherry*

WH1 ΔN37 — *mCherry* — pcDNA3.1-*repA-WH1(ΔN37)-mCherry*

B

	mCherry	WH1(WT)	WH1(A31V)	WH1(ΔN37)

N2a | HeLa | SH-SY5Y | N2a WH1(ΔN37) *pellet*

kDa

55 —

35 —

actin —

Fig. S1

A Electron microscopy

Unfragmented WH1(A31V) fibres Fragmented WH1(A31V) fibres

500 nm 500 nm
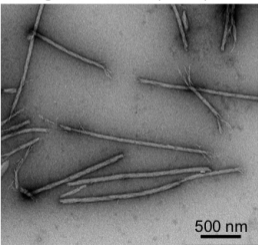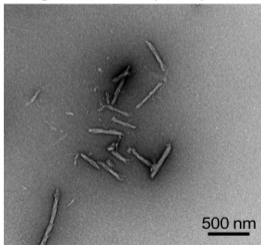
B Confocal microscopy

Fragmented WH1(A31V) fibres
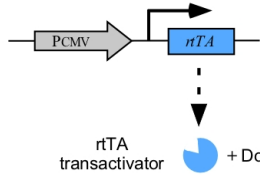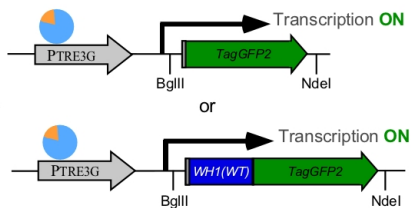
50 μm
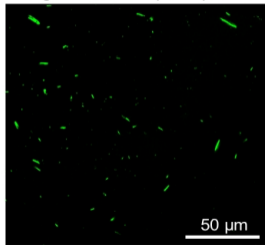
Fig. S2

A pCMV-Tet3G regulatory plasmid
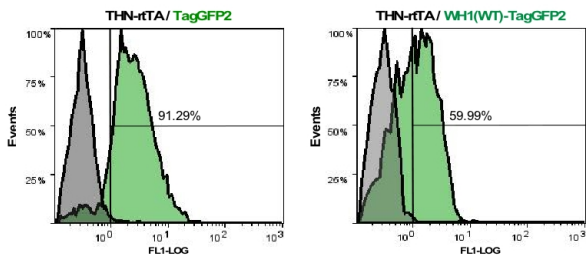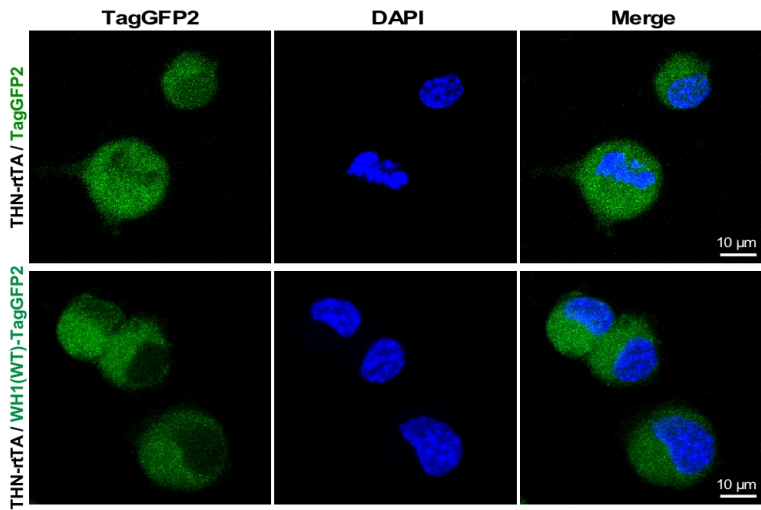
pTRE3G-WH1(Δ/WT/A31V)-**TagGFP2** response plasmids

B

C

D TagGFP2   DAPI   Merge
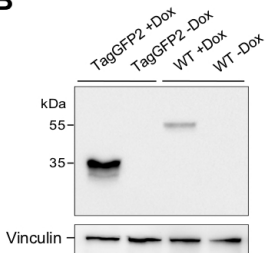
Fig. S3

A FIBRES-to-CELLS

108 (64.3%)   18 (10.7%)   42 (25.0%)
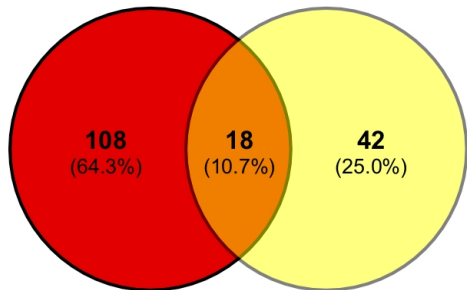
■ proteins in mCherry (R) cells + WH1(A31V) fibres
■ proteins in WH1(WT)-mCherry (R) cells + WH1(A31V) fibres

B CELLS-to-CELLS

44 (32.6%)   6 (4.4%)   85 (63.0%)
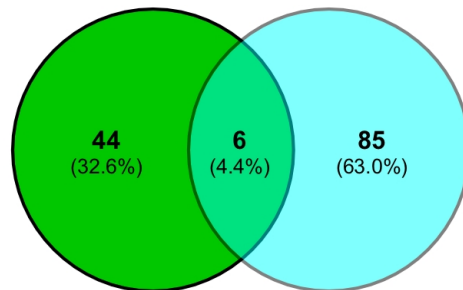
■ proteins in TagGFP2 (R) cells + WH1(A31V)-mCherry (D) cells
■ proteins in WH1(WT)-TagGFP2 (R) cells + WH1(A31V)-mCherry (D) cells

A panel network labels:
Complex I: Ndufs1, Acad9, Ndufb8, Ndufs3, Ndufs8, Ndufv1, Ndufs7, Ndufa11, Ndufv2, Ndufa9, Ndufb9, Ndufs2, Ndufb5, Ndufa5, Ndufa2, Ndufa6, Cox6c, Usmg5
Complex IV, Complex V
MITOCHONDRIA

Lepre1, Crtap, Emc7, Emc10, Isg15, Usp18, Dpp7, Hexb, Fbxo2, Ubr4, Atp6ap2 — protein quality control
Slc25a20, Crat, Acot2, Ech1 — fatty acids oxidation
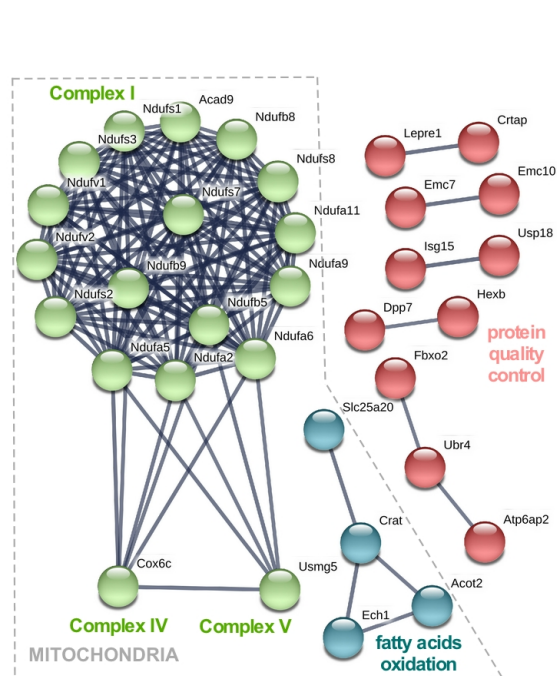
Highest confidence (0.9)
Interactions:
1st shell: ≤ 5
2nd shell: ≤ 10
MCL-means clusters: 3

B panel network labels:
protein quality control: PSMD6, CUL1
splicing: PRPF8, EFTUD2, SNRNP200
Complex I: NDUFA2, NDUFV2, NDUFV1, NDUFAB1, NDUFS6, NDUFS7, NDUFA6, NDUFB8, NDUFS2, NDUFS8, NDUFB7, NDUFA11, NDUFS3, NDUFB5, NDUFS1, NDUFA5
MITOCHONDRIA
exosomes: EXOSC8, DIS3, EXOSC3, MFGE8, COX5B
signaling: MLEC, SLC44A2, CD47, LAMTOR2, ATP6AP2, ITIH4
CLEC3B, TRMT6, TRMT61A, SRPR, SEC61A1, STT3B, STT3A
trafficking: DNAJC11, APOOL, PCYOX1L, SEC24C, COPB2, ARFGAP2, MIA3
glycoproteins & glycolipids: FUCA1, GM2A, ARSA, GCA, MAN2B1

Fig. S4